Probabilistic Engineering Mechanics 83 (2026) 103905

Contents lists available at ScienceDirect

Probabilistic Engineering Mechanics

journal homepage: www.elsevier.com/locate/probengmech

A spectrum-based ductility demand approach for the design of Fluid Viscous Dampers (FVDs) for the improvement of hysteretic framed r.c. structures under seismic excitations

Anthea Amato, Liborio Cavaleri *

Department of Engineering, University of Palermo, Italy

ARTICLE INFO

Keywords:
Fluid viscous dampers
Design strategy
Hysteretic structures
Seismic protection

ABSTRACT

Fluid viscous dampers (FVDs) have been widely used due to their capacity to generate dissipative forces (velocity dependent) that are not in phase with the displacements, namely able to exhibit their maximum forces when internal restoring forces are minimum. The possibility of increasing the damping ratio of a structure without significantly altering the inherent stiffness is another reason for the advantaging use of FVDs. For these characteristics, fluid viscous dampers are often preferred over other types of dampers. However, the lack of specific code prescriptions and simple but sufficiently reliable design procedures for structures exhibiting a non-linear plastic behavior is an issue not definitively faced. Deepening this issue could make the use of viscous dampers more diffused than it is. In this frame, here, a novel design procedure for non-linear FVDs to apply to hysteretic r.c. framed structures is proposed and discussed in terms of reliability in practical applications. The novelty of the procedure is that the scope of limiting the structural response is searched considering the contribution of external viscous damping, inherent viscous damping and hysteretic damping that the structure is able to exhibit. Therefore, the dimensioning of the external viscous dampers is carried out taking into account the rate of energy that the structure can dissipate by hysteretic damping differently from the most diffused approaches based on the maintaining of a structural elastic behavior. To this scope, the hypothesis of a simplified dynamic structural response is assumed to be coupled to the equivalent linearization of FVDs. The suitability of this hypothesis is discussed by a comparison between the obtainable results and the design targets in the case of structures that do not satisfy the assumed hypothesis. The results obtainable are analyzed in a statistical sense. Time history analyses of FVDs-equipped (and non) structural non-linear models are performed under appropriate families of base accelerograms. The design procedure is tested on benchmark models and on a case study in order to assess the degree of success of the proposed approach in connection to the assumed target objectives.

1. Introduction

Passive energy dissipation devices, such as viscous dampers or friction dampers, have been widely used in the last decades to limit the dynamic response of civil structures and infrastructures and to protect them from excessive internal forces or excessive ductility demand [1–31].

Among passive energy dissipation systems for civil structures and infrastructures, fluid viscous dampers (FVDs) have gained great interest thanks to the capability to dissipate, in part or totally, the energy of earthquakes by a velocity dependent behavior that leads to generating dissipative forces out of phase with displacements. The consequence of this mechanical behavior is a really contained influence on the structural inherent stiffness [32]. Design and distribution of FVDs are standardized in some current codes by simplified approaches (e.g. FEMA 356 [33]), really not dealing with the inherent non-linearity of structures (depending on damage). In different codes (e.g. Italian Technical Standards for Constructions [34]) the issue is not faced leaving the possibility to refer to documents of recognized accuracy and reliability. However, generally speaking, there is a strong tendency to deal with the dissipation of energy due to structural damage considering it as an equivalent damping inherent force or assuming that seismic energy can

This article is part of a special issue entitled: Stochastic Mechanics EMI 2023 published in Probabilistic Engineering Mechanics.

* Corresponding author. University of Palermo, Viale delle Scienze, Palermo, Italy.
E-mail address: liborio.cavaleri@unipa.it (L. Cavaleri).

https://doi.org/10.1016/j.probengmech.2026.103905
Received 17 November 2024; Received in revised form 8 December 2025; Accepted 19 February 2026
Available online 26 February 2026

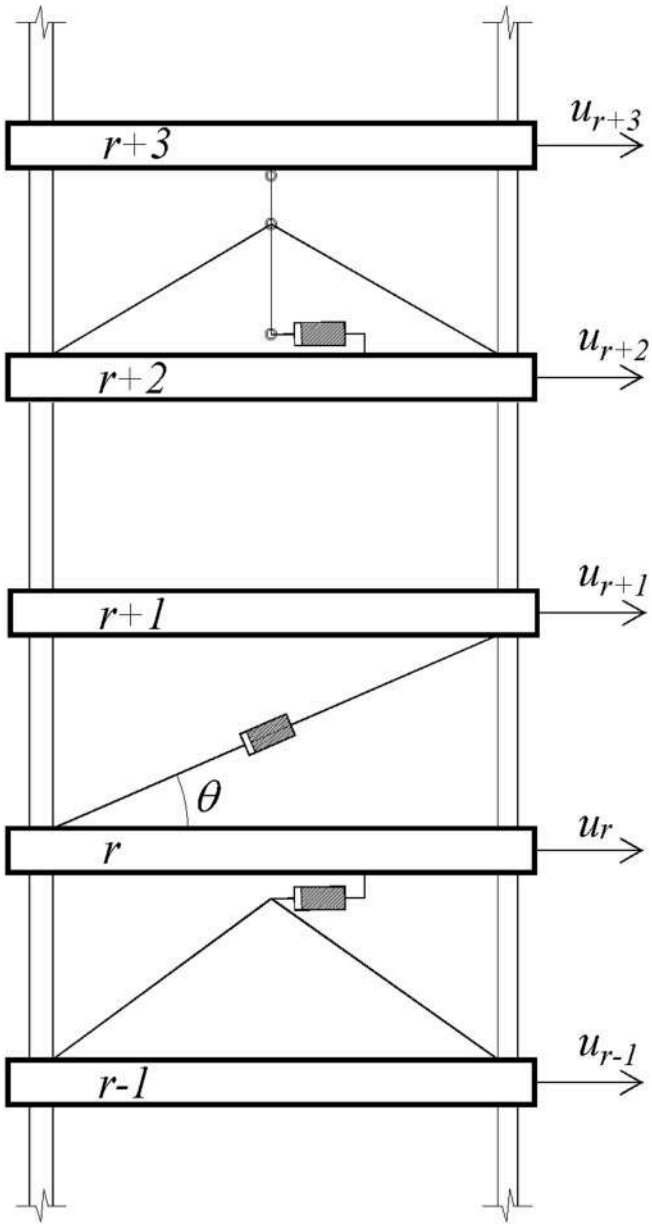

Fig. 1. – Scheme of a plane framed structure with three different damper arrangements: FVD coupled with K braces (between $(r-1)^{th}$ and r^{th} storey, with diagonal brace between r^{th} and $(r+1)^{th}$ storey, and coupled with a displacement amplification device between $(r+2)^{th}$ and $(r+3)^{th}$ storey (more details in Ref. [55]).

be dissipated by viscous damping maintaining the structure in an elastic stage (e.g., Refs. [35, 36]). Within the framework of the former strategy, different approaches based on an equivalent statistical linearization, so successful in the last three decades along with the equivalent statistical non-linearization (eg. Refs. [37, 38]) can also be found in the literature (eg,. Refs. [39, 40]). For both approaches, any complication due to the non-linearity of structures is overcome. This tendency is obviously connected with the sake of effective solutions for practical applications, able to give rapid responses to real problems, with a sufficient degree of approximation [25–31]. Among the different design strategies (heuristic, performance cost function minimizing approach, evolutionary by genetic algorithms), probably, the heuristic approach (the one used by the codes that discuss the FVDs design issue, as FEMA 356) is the most successful for practical applications. However, in the last two decades, optimization techniques and, in general, performance based approaches have been the object of different studies (e.g. Refs. [41–45]) revealing the effectiveness of these approaches, but also the need for further insights in connection with the choice of the function cost to be minimized. A similar remark holds for the approaches based on genetic algorithms (e.g. Refs. [46, 47, 48]).

The use of FVDs is not so diffused as it could be. This is due to the lack of extended code addresses and simple design procedures in the presence of structural non-linearities as well (this issue does not regard only FVDs). Further, the methods available in the literature are often not univocal and maintain a level of complexity that makes them not so open for practical applications.

Both for new constructions and for the enhancement/retrofitting of existing buildings, FVDs design requests the determination of optimal locations and corresponding capacities [49]. Then, the check of the effectiveness of capacities and locations can be done by high computational effort analyses because of the high non-linearity that often characterizes FVDs [50].

For new structures, FVDs' job is to prevent hysteretic dissipation and to make the system not exhibit plastic deformation, but in case of enhancement/retrofitting of structures often designed for vertical loads only, a damper system, designed trying to maintain low the costs, could be not sufficient to keep structural elements in the elastic range, therefore structural response under earthquake excitation has to be contained focusing on both reduction of ductility demand and increasing of viscous damping provided by the added dampers without renouncing to the inelastic energy dissipation capacity [50].

As regards the design approaches, some of them are specifically devoted to new structures (Palermo et al. [51] proposed a "five-step procedure" based on the identification of a target seismic performance such as, for example, a target damping ratio) while some others are devoted to existing structures (Marra et al. [52] proposed an approach based on energy dissipation demand, but specifically targeted for existing buildings).

In the case of structures to be built, it is necessary to design structure and dampers together. This issue is clear for example in Moradpour et al. [53] which proposed an optimal direct displacement-based design (DDBD) procedure for designing steel moment resisting frames equipped with non-linear fluid viscous dampers (FVDs). To solve the optimization problem, a genetic algorithm is used. The results showed a considerable reduction of the total damping coefficient needed and, hence, of the maximum dampers force.

The design approach proposed in this paper is heuristic and devoted to existing framed structures for which seismic capacity is associated to a combination of energy dissipation by inherent damping, additional damping provided by fluid viscous dampers and hysteretic behavior of structural members.

The novelty of the procedure is that the structural response is just limited considering the contribution of external viscous damping (possible by FVDs), inherent viscous damping and hysteretic damping that the structure can exhibit. Therefore, the dimensioning of the external viscous dampers is carried out taking into account the rate of energy that the structure can dissipate by hysteresis differently from the most diffused approaches based on the maintaining of the structural elastic behavior. This strategy reveals to be basic for existing structures to limit the costs of interventions (often due to the need of a high number of dissipation devices) simply by using the hysteretic structural capacity as effective for the scope to limit the seismic response and considering external viscous damping as complementary to that. In doing this, it is not renounced to the advantages of the linear analysis approaches.

Some simplifications, whose reliability and suitability are checked at the end of the design, are introduced. In details: i) an equivalent linear model of the structure is considered, whose equivalence is in terms of initial stiffness and displacement demand, ii) the dynamic response is assumed as governed by the first mode, iii) the damping due to the dampers is considered through an additional equivalent linear damping ratio (some other specifications are discussed through the paper).

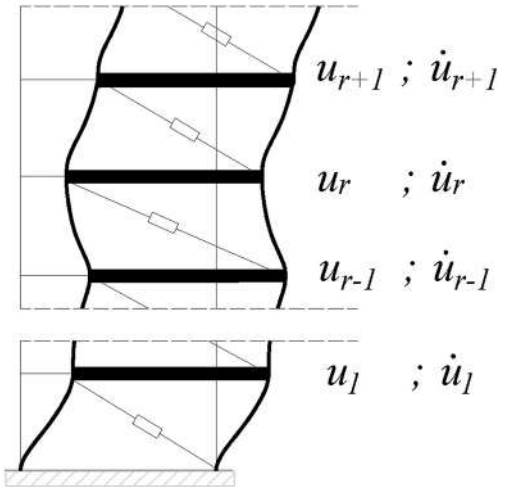

Fig. 2. – Scheme of a plane framed structure with displacement and velocity distribution.

However, it is very appropriate in practical applications, because of its simplicity for design and supporting analyses.

The n-degrees-of-freedom govern equation of a plane shear type system with fluid viscous dampers can be given by

$$\boldsymbol{M}\ddot{\boldsymbol{u}} + \boldsymbol{C}\dot{\boldsymbol{u}} + \boldsymbol{R}(\dot{\boldsymbol{u}}, \alpha) + \boldsymbol{F}(\boldsymbol{u}, \dot{\boldsymbol{u}}) = \boldsymbol{M}\boldsymbol{\tau}\ddot{u}_g \tag{2}$$

where **R** is the vector containing the forces transferred by the dampers to each storey because of the forces exhibited in the fluid viscous dampers. In an approximated approach, assuming that the damping force of the i-th floor (shear type scheme - Fig. 2) depends only on the velocities at the (1-1)-th, i-th and (i+1)-th storeys, and considering Eq. (1), each component of the vector **R** is

$$R_i = C_i l_i^{\alpha} |\dot{u}_i - \dot{u}_{i-1}|^{\alpha} \mathrm{sgn}(\dot{u}_i - \dot{u}_{i-1}) + C_{i+1} l_{i+1}^{\alpha} |\dot{u}_{i+1} - \dot{u}_i|^{\alpha} \mathrm{sgn}(\dot{u}_{i+1} - \dot{u}_i) \tag{3}$$

In Eq. (2), **F** is the vector containing the restoring hysteretic forces, while **C** is the matrix of the inherent damping and **τ** is the n-dimensional influence vector in which each component is 1 for plane systems.

If the parameter α is equal to 1, the vector ***R*** can be simply expressed as

$$\mathbf{R}(\dot{\mathbf{u}}, \alpha = 1) = \begin{bmatrix} C_1 + C_2 & -C_2 & 0 & & & & 0 \\ -C_2 & C_2 + C_3 & -C_3 & 0 & & & 0 \\ 0 & -C_3 & C_3 + C_4 & -C_4 & 0 & & 0 \\ \dots & \dots & \dots & \dots & \dots & \dots & \dots \\ \dots & \dots & \dots & \dots & \dots & \dots & \dots \\ & & & & -C_{n-1} & C_{n-1} + C_n & -C_n \\ 0 & & & & & -C_n & C_n \end{bmatrix} \mathbf{T} \begin{bmatrix} \dot{u}_1 \\ \dot{u}_2 \\ .. \\ .. \\ .. \\ .. \\ \dot{u}_n \end{bmatrix} \tag{4}$$

However, the concept of structural hysteretic dissipation is strong from the beginning of the proposed procedure: the additional damping ratio is fixed depending on a comparison between the actual ductility capacity of the structure (predicted by a pushover analysis) and the ductility demand obtained using the response spectra (of accelerations and displacements) in agreement to the method N2 [54]. Once the additional linear damping ratio is defined, the non-linear engineered parameters are obtained for the damper commissioning as detailed hereinafter.

2. Models assumed for fluid viscous dampers' forces

The functioning of a fluid viscous damper is influenced by many factors. However, it is generally a cylinder-piston system exhibiting forces depending on the relative velocity between the ends of cylinder and piston. In brief, this force can be expressed as a function of a constant and the power of the relative piston-cylinder velocity. For the i-th interstorey location (Fig. 1) the damper force f_i is expressed as:

$$f_i = C_i \cdot |l_i(\dot{u}_i - \dot{u}_{i-1})|^{\alpha} \cdot \mathrm{sgn}(\dot{u}_i - \dot{u}_{i-1}) = C_i l_i^{\alpha} |(\dot{u}_i - \dot{u}_{i-1})|^{\alpha} \cdot \mathrm{sgn}(\dot{u}_i - \dot{u}_{i-1}) \tag{1}$$

In Eq. (1), $(\dot{u}_i - \dot{u}_{i-1})$ is the interstorey velocity, C_i and α are constants depending on the constructive characteristics (fluid and piston properties) of the damper and having the role explained hereinafter, finally, $\mathrm{sgn}(\cdot)$ is the "signum" function and l_i is a transformation factor, useful for transforming the interstorey velocity in the relative velocity between the ends of cylinder and piston ($l_i = 1$ in the case of K support braces and $l_i = \cos\theta$ in the case of diagonal support brace having slope θ). For civil applications, it is frequent to find α assuming values in the range 0.15-0.5.

The model (1) is not considered the most advanced (more advanced models are based on the use of fractional derivatives– e.g. Ref. [56]). that assumes a basic significance in the dampers design procedure.

In Eq. (4) **T** is an nxn transformation diagonal matrix whose i-th term is the transformation factor l_i. Also, C_1, C_2, … C_n are the constant coefficients characterizing the fluid viscous dampers at each storey in agreement to Eq. (1).

In order to highlight the physical meaning of the parameters C_i and α appearing in Eq. (1), in Fig. 3 the force-displacement curves of a fluid viscous damper varying the parameter C_i $\left(C_i = \frac{100}{\pi}, \frac{200}{\pi}, \frac{400}{\pi}\ \frac{kN\ \mathrm{sec}}{cm}\right)$, interested by a sinusoidal history of displacements and characterized by $\alpha = 1$ are shown. Further, the cycles described reducing the value of α from 1 to 0.15, and contemporarily increasing the parameter C_i in such a way to maintain constant the maximum dissipative force, are shown.

From these curves, it is clear that the role of the parameter C is to increase the maximum dissipative force and of obtain a higher dissipated energy. Further, the parameter α modifies the shape of the cycle: for smaller values of α the cycle is closer to a rectangle, instead, in the case of linear behavior ($\alpha = 1$) the shape of the curve is an ellipse. As soon as the cycle approximates a rectangle, a higher level of the dissipative forces can be obtained just for low levels of the velocities.

As the parameter α tends to zero, the limit condition is characterized by the same value of dissipative force at each velocity (rectangular force-displacement cycle). Therefore, the reduction of the parameters α makes the fluid viscous damper exhibit a behavior close to that of a friction damper.

It is worth underlining that, when the maximum dissipative force is fixed, a reduction in the value of α requests an increase of the value of C.

3. Estimation of the additional damping for a system having ductility capacity lower than ductility demand

In agreement with N2 method [54], in a high number of cases, multi

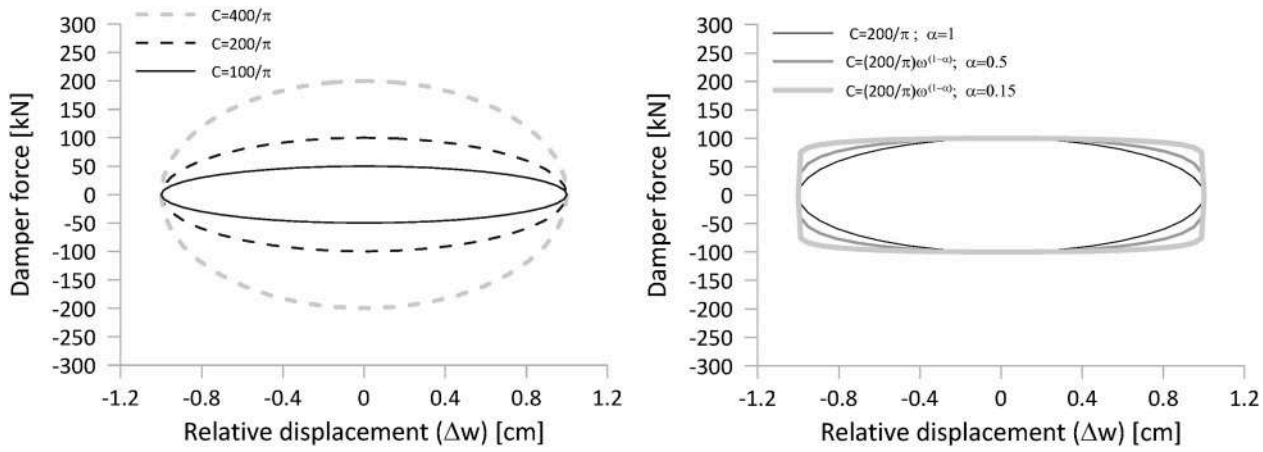

Fig. 3. Force displacement curves of dampers with different characteristics: a) α = 1, C = variable; b) C = variable, α = variable.

degrees of freedom (MDOF) systems can be transformed into single degree of freedom (SDOF) systems with elastic perfect plastic behavior. In these cases a safety check in terms of ductility can be done. In doing this, the equation of motion of the equivalent SDOF system is

$$m\ddot{\delta} + m2\varsigma\omega\dot{\delta} + F(\delta,\dot{\delta}) = -m\ddot{\delta}_g \tag{5}$$

where m is the equivalent mass, $\ddot{\delta}, \dot{\delta}, \delta$ are acceleration, velocity and displacement of the equivalent SDOF equivalent, F is the restoring force, ζ and ω are damping ratio and frequency of the unforced and undamped free oscillations. It is proved that the following relations hold

$$m = \boldsymbol{\phi}_1^T\mathbf{M}\tau;\ \ \delta = D\Big/\Gamma;\ \ \Gamma = \frac{\boldsymbol{\phi}_1^T\mathbf{M}\boldsymbol{\tau}}{\boldsymbol{\phi}_1^T\mathbf{M}\boldsymbol{\phi}_1};\ F = V\Big/\Gamma \tag{6}$$

Being $\boldsymbol{M}$ the mass matrix, D the displacement of a control point (usually at roof level) and Γ the participation factor of the main eigenvector along the direction of the seismic loading (that is $\boldsymbol{\phi_1}$).

The representation of a monotonic bilinear equivalent form of the F-δ curve is shown in Fig. 4.

From Fig. 4 it is possible to derive the available ductility of the system μ_a, that has to be compared with the ductility demand μ_d. The expressions are

$$\mu_a = \frac{\delta_{ua}}{\delta_e}, \mu_d = \frac{\delta_{ud}}{\delta_e} \tag{7}$$

From the comparison of the expressions of μ_a and μ_d, it emerges that what is decisive in the ductility check is the comparison between the capacity in terms of ultimate displacement (δ_{ua}) and the corresponding

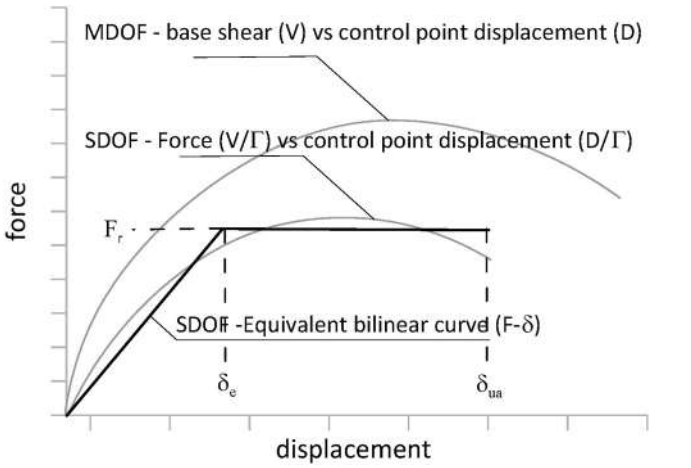

Fig. 4. –Bilinear F-δ curve of the equivalent SDOF system.

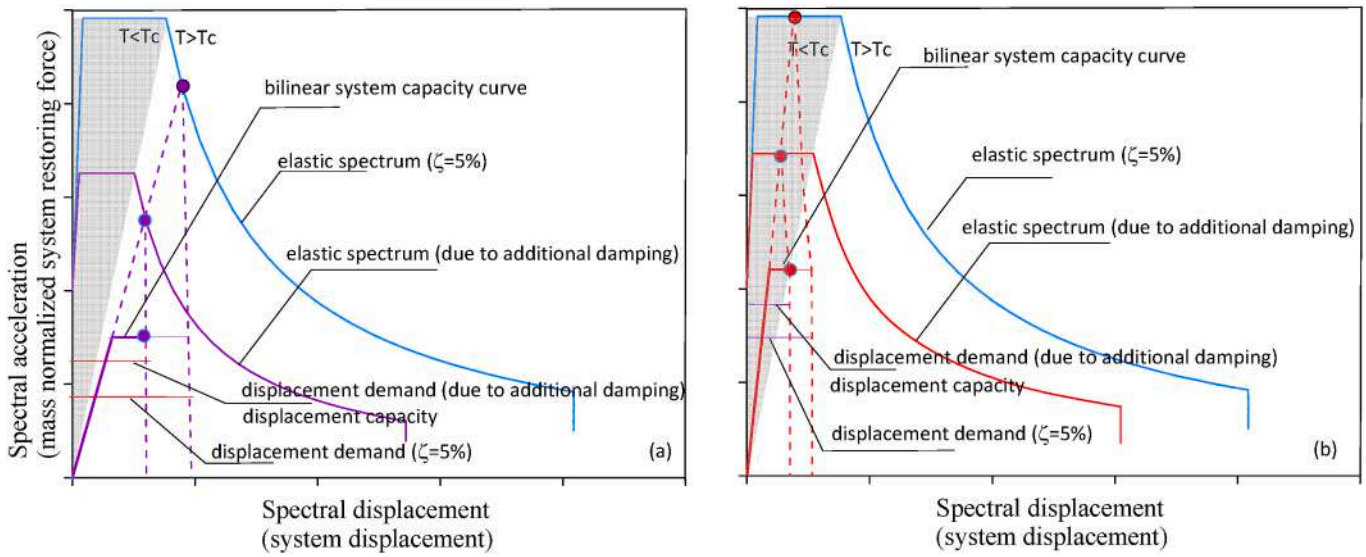

Fig. 5. Graphical estimation of the additional damping approach: a) T*>Tc, b) T*<Tc.

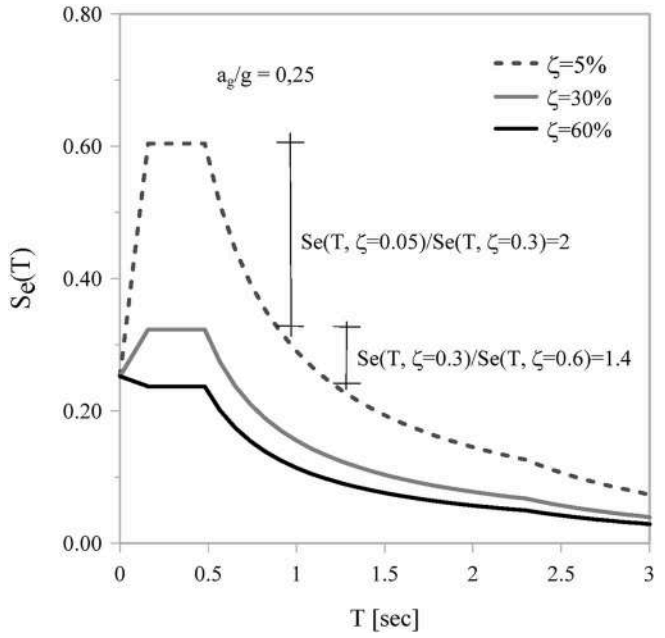

Fig. 6. – Elastic spectrum accelerations for different values of damping ratio.

demand (δ_{ud}).

The strength F_r of the equivalent bilinear SDOF system, compared to the strength required for an elastic linear system (in agreement to the pseudo-acceleration response spectrum), provides the strength reduction factor R_μ, that is

$$R_\mu = \frac{mS_e(T^*)}{F_r} = \frac{\delta_e^*}{\delta_e} \tag{8}$$

where δ_e^* is the displacement demand for the elastic linear system having the same stiffness of the bilinear SDOF one in its linear branch. Now, the correlations between the displacement demands for an elastic linear system and an elastic perfect plastic system characterized by a strength reduction factor R_μ, in the two period domains $0 \le T^* < T_C$ and $T^* \ge T_C$, are expressed by

$$\delta_e^* = \delta_e\left(\frac{\delta_{ud}}{\delta_e} - 1\right)\frac{T^*}{T_C} \quad or \quad R_\mu = \left(\frac{\delta_{ud}}{\delta_e} - 1\right)\frac{T^*}{T_C} + 1; \quad 0 \le T^* < T_C \tag{9-a}$$

$$\delta_e^* = \delta_{ud} \quad or \quad R_\mu = \frac{\delta_{ud}}{\delta_e}; \quad T^* \ge T_C. \tag{9-b}$$

where T* is the natural period consistent with the linear branch of the equivalent bilinear SDOF system, while T_C is the period between the constant acceleration plateau and the constant velocity branch of the response spectrum.

The correlations between the displacement demands in Eqs (9) have a statistical meaning, that is, Eqs (9) are valid in average based on a high number of analyses [54]. Surely, the statistical equivalence between the linear SDOF system and the elastic perfect plastic non-linear one used hereinafter is not as strong as in other studies specifically addressed to the statistical equivalence between non-linear and linear behaviour [e.g., 39 and 40]. However, it may have the advantage of encountering a large use in connection with the wide diffusion of the N2 method in different standard codes [e.g. 34].

Eqs 9-a and 9-b allow to predict the displacement demand δ_{ud} once the strength reduction factor is known. Considering Eq. (8), the dependence of $S_e(T^*)$ on the damping ratio ς and substituting $\frac{\delta_{ud}}{\delta_e}$ with the available ductility $\frac{\delta_{ua}}{\delta_e}$, Eqs.9 can be rewritten as

$$\frac{mS_e(T^*, \xi_{eff})}{F_r} = \left(\frac{\delta_{ua}}{\delta_e} - 1\right)\frac{T^*}{T_C} + 1; \quad 0 \le T^* < T_C \tag{10-a}$$

$$\frac{mS_e(T^*, \xi_{eff})}{F_r} = \frac{\delta_{ua}}{\delta_e}; \quad T^* \ge T_C \tag{10-b}$$

in which the damping ratio ξ_{eff}, corresponding to a ductility demand fixed equal to the ductility capacity, appears as unknown: therefore, solving Eqs (10) with respect to the unknown ξ_{eff} means to determine the best additional damping ξ_d for the structural retrofitting, being

$$\xi_{eff} = \xi_d + \xi \tag{11}$$

where ξ is the inherent damping ratio of the structure in the state before the enhancement.

Fig. 5, in which the response spectrum in the acceleration-displacement plane is represented, helps to understand the core of the additional damping estimation approach.

4. Design strategy for external linear FVDs based on the additional damping system request

In this section the procedure proposed to design the FVDs for an existing hysteretic structure is discussed. The characteristics of the FVDs for improving the structural seismic behaviour are defined referring to the elastic response spectrum and the linear SDOF system associated with the actual structure in the linear state, and the correlation between the behaviour of the linear elastic SDOF system before mentioned and elastic-plastic SDOF system, equivalent to the structure to be improved, characterized by the strength reduction factor R_μ. Starting from the additional damping ratio necessary to obtain the correspondence between displacement demand and displacement capacity (see previous section) the characteristics of the linear FVDs can then analytically derived. In doing this, the strength F_r of the equivalent bilinear system, necessary to solve Eqs (10) can be estimated by a preliminary pushover analysis, in agreement to the N2 method before mentioned.

The additional damping ratio ξ_d to be introduced by FVDs is obtainable by Eq. (11) once Eqs.(10) are solved considering that the inherent damping ratio ξ generally attributed to framed structures is in the range 0.03-0.05. The next step is the correlation of the additional damping needed with an appropriate number and distribution of FVDs. In this stage, it is worth highlighting that it is not reasonable to increase the overall damping ratio over 30% because, after this value, the improvement of the structural behavior strongly reduces not justifying the major cost for the FVDs. This circumstance is visible in Fig. 6 in which it is possible to observe that an increase in the global damping ratio from 5% to 30% causes a force reduction higher than an increase from 30% to 60%, especially in the range of periods higher than T_c.

In order to provide a first estimation of parameters needed to size FVDs in existing structures, it is possible to perform simplified analyses. It is hypothesized that the structure has a plane shear type behaviour, as shown in Fig. 2.

If on one hand, by the constructive point of view, FVDs are characterized by the model (1) with the parameter α generally not higher than 0.5, on the other hand, in this stage of the design, in order to reduce the computational effort, it is supposed to introduce linear equivalent FVDs, namely characterized by $\alpha = 1$. It is assumed a uniform distribution of FVDs in elevation of the structure and the coincidence of the FVDs' velocity and the interstorey velocity (possible in the case of FVDs on K braces – ref. Fig. 1).

Under this hypothesis, Eq. (2), can be rewritten as:

$$\mathbf{M}\ddot{\mathbf{u}}(t) + \mathbf{C}^{(S)}\dot{\mathbf{u}}(t) + \mathbf{C}^{(D)}\dot{\mathbf{u}}(t) + \mathbf{K}\mathbf{u}(t) = -\mathbf{M}\boldsymbol{\tau}\ddot{x}_g(t) \tag{12}$$

where $\mathbf{C}^{(S)}$ is the structural inherent damping matrix and $\mathbf{C}^{(D)}$ is the damping matrix associated to the FVDs.

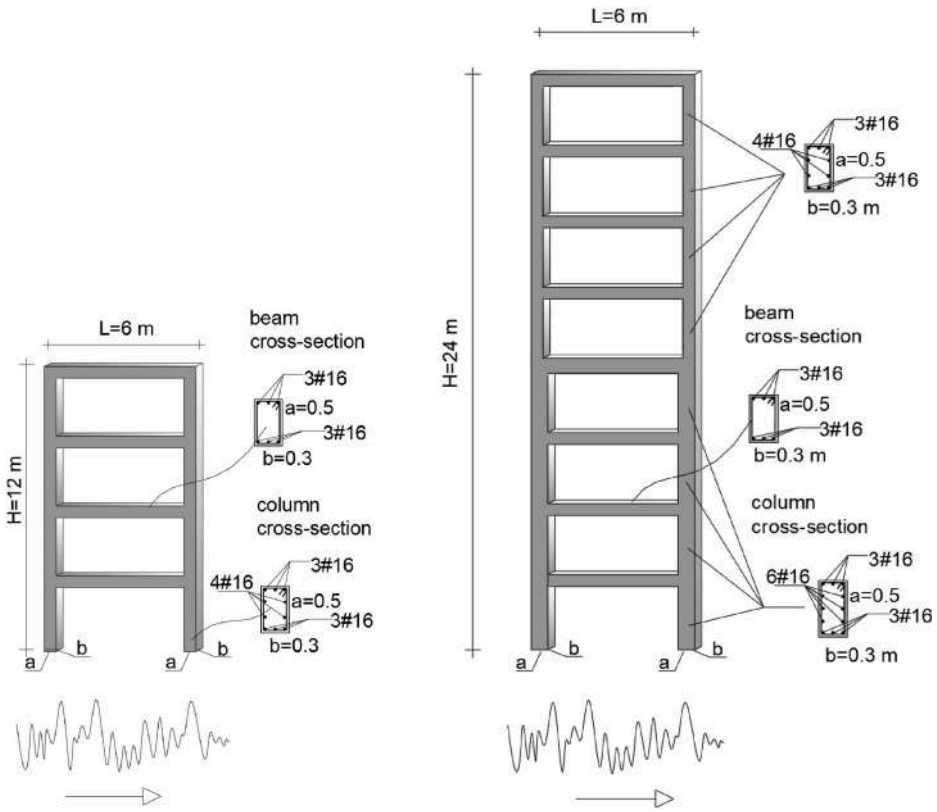

Fig. 7. – Plane benchmark models for the probabilistic reliability assessment for the proposed procedure: a) low-rise structure characterized by a plane behaviour; b) mid-rise structure characterized by a plane behaviour.

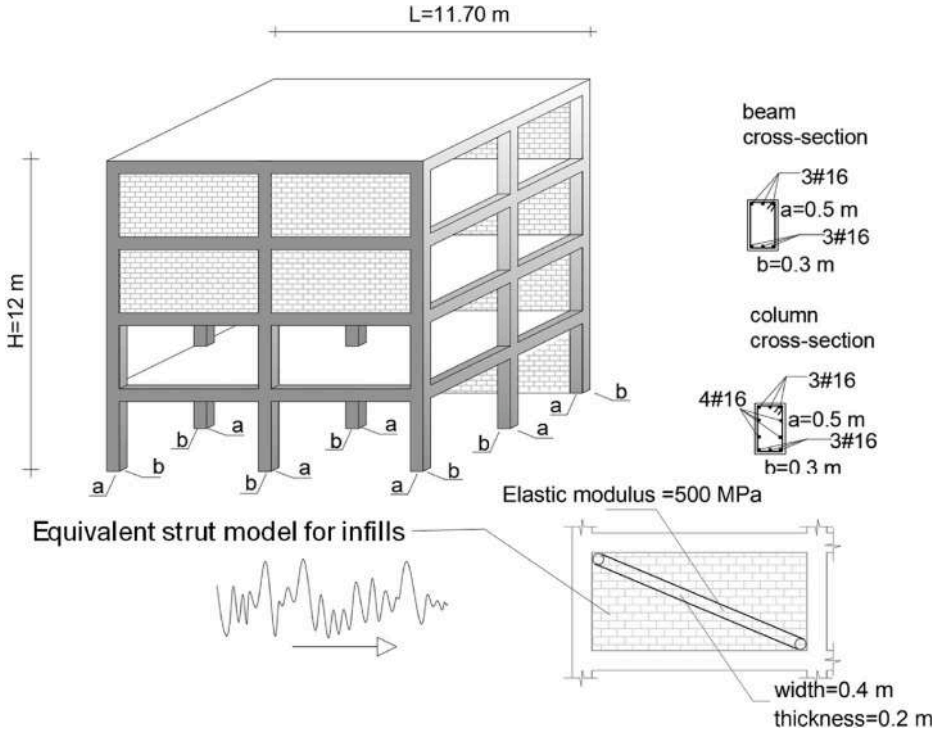

Fig. 8. – Irregular benchmark structure for the probabilistic reliability assessment of the proposed procedure.

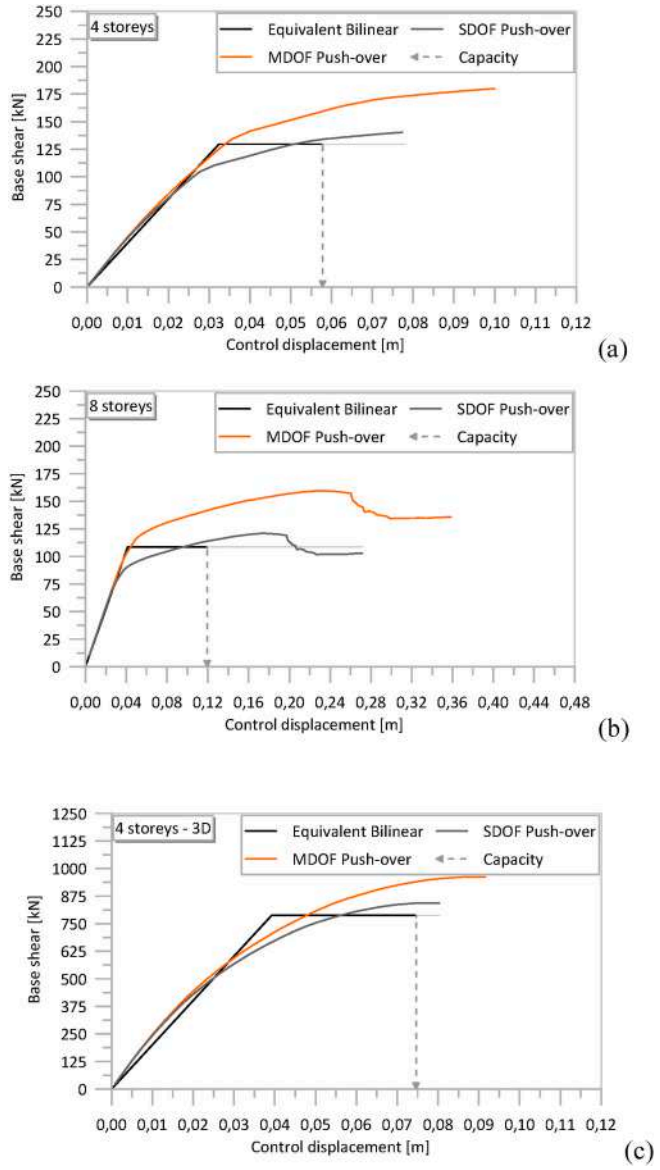

Fig. 9. – MDOF, SDOF and Bilinear structural responses of the three benchmark models.

If it is assumed that the dissipation capacity is constant at each storey and that it is defined by the scalar parameter C, the matrix $\mathbf{C}^{(D)}$, under the assumption of shear type behaviour, becomes (the first line refers to the lowest storey):

$$\mathbf{C}^{(D)} = C \cdot \mathbf{P} = C \cdot \begin{bmatrix} 2 & -1 & 0 & .. & .. & .. & 0 \\ -1 & 2 & -1 & 0 & .. & .. & 0 \\ 0 & -1 & 2 & -1 & 0 & .. & 0 \\ .. & .. & .. & .. & .. & .. & .. \\ 0 & .. & 0 & -1 & 2 & -1 & 0 \\ 0 & .. & .. & 0 & -1 & 2 & -1 \\ 0 & .. & .. & .. & 0 & -1 & 1 \end{bmatrix} \tag{13}$$

If it is assumed that the structural response is governed by the first eigenvector, that is

$$\mathbf{u}(t) = \boldsymbol{\phi}_1 y_1(t); \quad \dot{\mathbf{u}}(t) = \boldsymbol{\phi}_1 \dot{y}_1(t) \tag{14}$$

in which $\boldsymbol{\phi}_1$ is the eigenvector, associated to the lowest circular frequency ω_1, and $y_1(t)$ is the modal coordinate of the first vibration mode, then Eq. (12) can be rewritten as:

$$\ddot{y}_1(t) + (2\xi\omega_1 + 2\xi_d\omega_1)\dot{y}_1(t) + \omega_1^2 y_1(t) = g_1 \ddot{x}_g(t) \tag{15}$$

in which

$$g_1 = -\frac{\boldsymbol{\phi}_1^T \mathbf{M} \boldsymbol{\tau}}{\boldsymbol{\phi}_1^T \mathbf{M} \boldsymbol{\phi}_1}; \quad \omega_1^2 = \frac{\boldsymbol{\phi}_1^T \mathbf{K} \boldsymbol{\phi}_1}{\boldsymbol{\phi}_1^T \mathbf{M} \boldsymbol{\phi}_1}; \quad 2\xi\omega_1 = \frac{\boldsymbol{\phi}_1^T \mathbf{C}^{(S)} \boldsymbol{\phi}_1}{\boldsymbol{\phi}_1^T \mathbf{M} \boldsymbol{\phi}_1} \tag{16}$$

and

$$2\xi_d\omega_1 = \frac{\boldsymbol{\phi}_1^T \mathbf{C}^{(D)} \boldsymbol{\phi}_1}{\boldsymbol{\phi}_1^T \mathbf{M} \boldsymbol{\phi}_1} \tag{17}$$

Comparing Eq. (13) and Eq. (17) leads to

$$2\xi_d\omega_1 = C \frac{\boldsymbol{\phi}_1^T \mathbf{P} \boldsymbol{\phi}_1}{\boldsymbol{\phi}_1^T \mathbf{M} \boldsymbol{\phi}_1} \tag{18}$$

Then, from Eq. (18), it simply derives the following Eq. (19):

$$C = 2\xi_d\omega_1 \frac{\boldsymbol{\phi}_1^T \mathbf{M} \boldsymbol{\phi}_1}{\boldsymbol{\phi}_1^T \mathbf{P} \boldsymbol{\phi}_1} \tag{19}$$

The parameter C obtained from Eq. (19), is representative of the dissipation provided by all the FVDs at one storey in one direction. If s dampers per storey are installed, each of them will be characterized by a dissipation constant C_i

$$C_i = \frac{C}{s} \tag{20}$$

Although not consistent with the initial assumption, an attempt of a different distribution (for example in the case of tall structures where the relative velocity at each storey can be very different along the eight) can be tried after the assessment of the overall dissipation parameter C*, that is

$$C^* = nC, \tag{21}$$

where C, as mentioned before, is the dissipation constant associated to the i-th storey and n is the number of storeys, and redistributing the

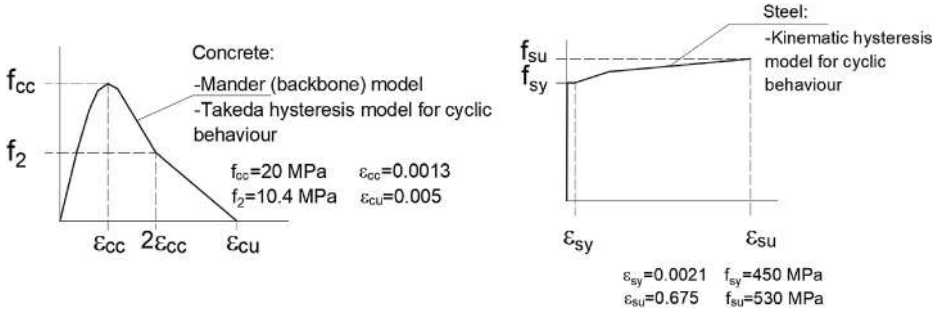

Fig. 10. – Mechanical cyclic behaviour of concrete and steel used for the cross-sections.

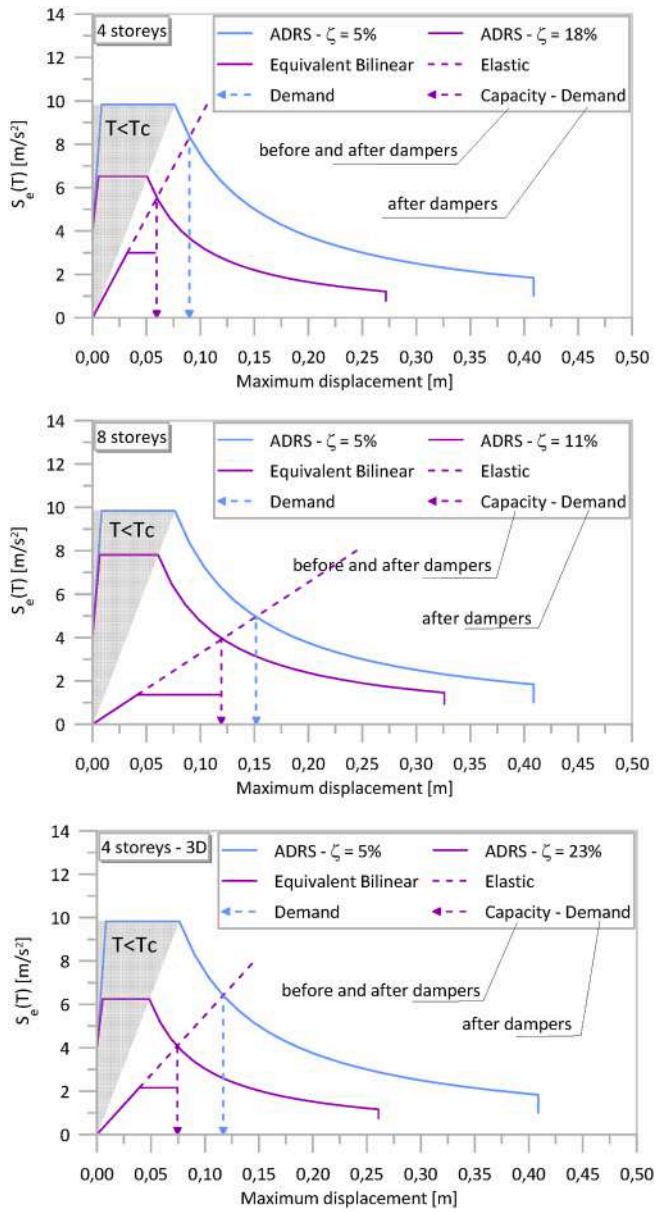

Fig. 11. – Bilinear structural responses (mass normalized) and acceleration-displacement response spectra (PGA = 0.41g) before (ζ = 5%) and after the introduction of fluid viscous dampers – nominal capacity-demand ratio in the original state 0.7.

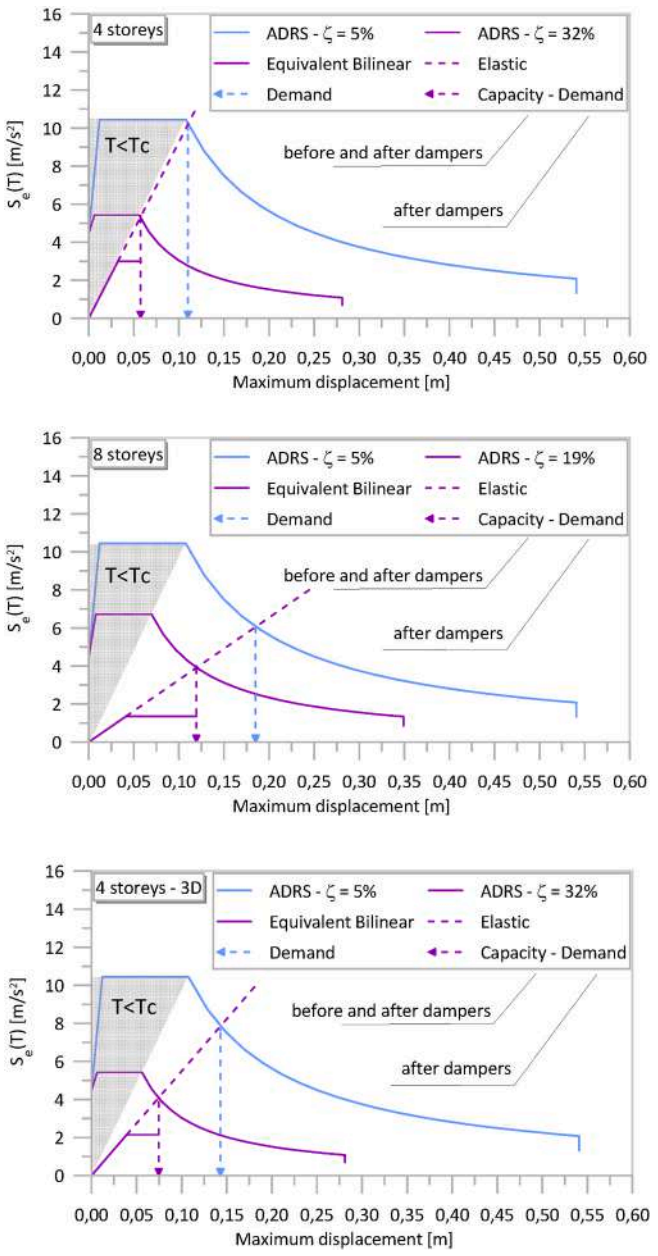

Fig. 12. – Bilinear structural responses (mass normalized) and acceleration-displacement response spectra (PGA = 0.46g) before (ζ = 5%) and after the introduction of fluid viscous dampers – nominal capacity-demand ratio in the original state 0.5.

overall dissipating capacity in agreement to a different criterium. It can be simply proved that a distribution proportional to the storey shear is obtained by using the distribution coefficient

$$S_i = \frac{\frac{m_i}{\phi_{1i}}}{\sum_{i=1}^{n} \frac{m_i}{\phi_{1i}}} \tag{22}$$

Eq. (22) can be further simplified if it is assumed the simplified linear distribution of the components of the first eigenvector, that is

$$\phi_{1i} = ch_i \tag{23}$$

where h_i is the distance of the i-th storey from the ground while c is a constant coefficient. Substituting Eq. (23) in Eq. (22) leads to

$$S_j = \frac{\frac{m_j}{h_j}}{\sum_{i=1}^{n} \frac{m_i}{h_i}} \tag{24}$$

Then considering Eq. (24) and Eq. (21) the damper constant C_j associated to the i-th storey becomes

$$C_j = C^* \frac{\frac{m_j}{h_j}}{\sum_{i=1}^{n} \frac{m_i}{h_i}} \tag{25}$$

Hereinafter, each time a distribution of dampers consistent with the distribution of shear in elevation will be referred to, the simplified Eq. (25) will be used.

Eq. (19) is equivalent to the simplified formula proposed by FEMA

Table 1
– Values of the additional damping ζ_d and the corresponding FVDs' parameters, and the participation mass associated to the modal shape used for the design.

PGA [g]	ζ_d [%]		$C_{lc}\left[kN\cdot\frac{s}{m}\right]$		$C_{nlc}\left[kN\cdot\left(\frac{s}{m}\right)^{0.15}\right]$	
	0,41	0,46	0,41	0,46	0,41	0,46
4 Storeys	13	27	384	828	70	149
8 Storeys	6	14	317	740	39	91
4 Storeys – 3D	18	27	840	1261	137	206

PGA [g]	$C_{lp}\left[kN\cdot\frac{s}{m}\right]$				$C_{nlp}\left[kN\cdot\left(\frac{s}{m}\right)^{0.15}\right]$				Participating Mass
	0,41		0,46		0,41		0,46		
4 Storeys	Bottom/Top Storey		Bottom/Top Storey		Bottom/Top Storey		Bottom/Top Storey		
	738	184	1590	397	134	33	286	71	84%
8 Storeys	939	114	2192	266	115	14	2693	33	78%
4 Storeys – 3D	1614	403	2421	605	263	65	395	99	79%

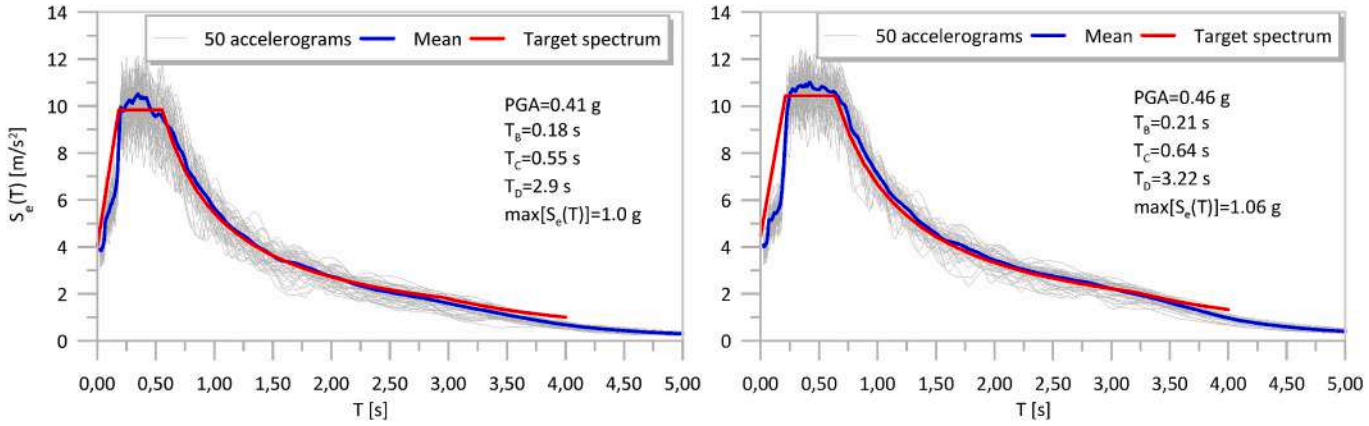

Fig. 13. – Comparison between target spectra and spectra of the accelerograms used for the dynamic analyses (Target spectra parameters in figure; T_B: period at the beginning of the response spectrum plateau, T_D: period between the constant velocity branch and the constant displacement branch).

356 [33]. However, here, differently from there, ξ_d has the stronger meaning of supplemental damping ratio for a system under a seismic action characterized by a specific response spectrum, and able to exhibit a non-linear behavior due to the plasticization of its members.

5. Design strategy for non-linear FVDs

A rapid assessment of the i-th dissipation constant C_i characterizing the i-th FVD is possible only in the case of linear damper behaviour. However a higher effectiveness of the fluid viscous dampers depends on the possibility to be activated for low velocities. This is possible if an almost rectangular force-displacement cycle ($\alpha \leq 0.3$) is obtained. Once obtained the constant (C_l) associated to a linear dissipation, there are different methods to pass from the latter to a constant (C_{nl}) suitable for a non-linear behaviour. The most successful is based on the equivalence of the dissipated energies over a displacement cycle.

In this case, the correlation between the coefficients C_l and C_{nl} is obtained as [57,58].

$$C_{nl} = \frac{C_l \cdot \left(|\dot{x}|_{\max}\right)^{1-\alpha}}{\lambda} \tag{26}$$

where $|\dot{x}|_{\max}$ is the maximum absolute value of the damper velocity while λ is equal to:

$$\lambda = \frac{\left[2^{2+\alpha}\cdot\Gamma^2\left(1+\frac{\alpha}{2}\right)\right]}{\pi\cdot\Gamma(2+\alpha)} \tag{27}$$

where Γ is the gamma function. Eq. (26) is based on the assumption that the maximum velocity exhibited by a linear damper is equal to the maximum velocity exhibited by a non-linear damper. However, in general, it is a not true condition that may lead to an ineffective distribution of the non-linear dampers.

The value of the coefficient λ assumes values greater than 1. It is tabulated in Code FEMA 273 and 274 as a function of α. When the coefficient α approaches zero, that means that the damper force-displacement cycle approaches a rectangle, then the value of λ approaches to $4/\pi$. The maximum variation of λ from $\alpha = 0$ to $\alpha = 0.3$ is of 8%. Therefore, it is reasonable to use a constant value of λ in the range of α mentioned above that can be just $4/\pi$. In this case, Eq. (26) becomes simply

$$C_{nl} = \frac{C_l \cdot |\dot{x}_{\max}|^{(1-\alpha)}}{4/\pi} \tag{28}$$

A simplified approach in the estimation of $|\dot{x}_{\max}|$ is possible if it is assumed a linear distribution of the storeys' velocities. This assumption leads to a uniform distribution of the dampers' velocities, that is

$$C_{nl} = \frac{C_l \cdot \left(|\dot{u}_{n,\max}|/n\right)^{(1-\alpha)}}{4/\pi} \tag{29}$$

where $u_{n,\max}$ is the maximum velocity at the top storey. Considering the equivalence between elastic and elastic plastic SDOF system, it can be estimated from the velocity spectrum, that is

$$|\dot{u}_{n,\max}| = p_1 S_v(T^*) = \frac{g_1 S_e(T^*)}{2\pi} T^* \tag{30}$$

where T* is the period of the elastic plastic equivalent SDOF system, in its elastic stage, obtained in agreement to the N2 method, and g_1, as

Table 2
– Mean and standard deviation of the capacity-demand ratios obtained from 50 dynamic analyses.

		Capacity/Demand							
		mean				standard deviation			
4 Storeys	Inherent Damping (5%)	C/D = 0.7 from N2	0,625	C/D = 0.5 from N2	0,485	C/D = 0.7 from N2	0,071	C/D = 0.5 from N2	0,059
	Additional Inherent Damping (13% and 27%)	method	1338	method	1585	method	0,182	method	0,180
	linear FVDs – uniform distribution		1288		1,52		0,237		0,267
	nonlinear FVDs – uniform distribution		1700		3030		0,384		0,641
	linear FVDs – storey shear distribution		1344		1585		0,191		0,179
	nonlinear linear FVDs – storey shear distribution		1814		3459		0,380		0,697
8 Storeys	Inherent Damping (5%)	C/D = 0.7 from N2	0,742	C/D = 0.5 from N2	0,461	C/D = 0.7 from N2	0,330	C/D = 0.5 from N2	0,156
	Additional Inherent Damping (6% and 15%)	method	1085	method	0,891	method	0,368	method	0,359
	linear FVDs – uniform distribution		0,976		0,696		0,374		0,336
	nonlinear FVDs – uniform distribution		1082		0,700		0,395		0,398
	linear FVDs – storey shear distribution		1139		1103		0,303		0,240
	nonlinear linear FVDs – storey shear distribution		1300		1290		0,209		0,202
4 Storeys – 3D	Inherent Damping (5%)	C/D = 0.7 from N2	0,812	C/D = 0.5 from N2	0,656	C/D = 0.7 from N2	0,103	C/D = 0.5 from N2	0,098
	Additional Inherent Damping (18% and 27%)	method	1348	method	1299	method	0,246	method	0,226
	linear FVDs – uniform distribution		1297		1239		0,240		0,216
	nonlinear FVDs – uniform distribution		1427		1429		0,332		0,336
	linear FVDs – storey shear distribution		1350		1300		0,255		0,239
	nonlinear linear FVDs – storey shear distribution		1511		1549		0,353		0,376

mentioned before, is the participation factor associated to mode shape that has allowed the definition of the SDOF equivalent system.

6. Reliability of the proposed design strategy

In this section, the reliability of the proposed FVDs' design strategy is proposed in a probabilistic sense. Three different benchmark structures are considered, two of them having a plane behavior (Fig. 7), that is coherent with the assumptions at the base of the design strategy in question, and one characterized by an irregular-in plan behaviour (Fig. 8), that is far from the before mentioned assumptions. The test on these three benchmark structures is considered basic to prove the reliability of the proposed strategy just for the numerous simplified assumptions. In different cases, the characteristics encountered in the practical applications may differ from those used to define the approach discussed. Therefore, an observation of the results from different classes of structures, not necessarily complying with the assumptions, has the scope to be aware of the applicability of the proposed procedure. Here, the classes of low-rise plane structures (having the closest characteristics to the assumptions), mid-rise plane structures (in which the first mode shape does not comply with Eq. (24)) and in-plan irregular structures (the plane behavior is one of the basic assumptions) have been investigated.

The plane four storeys structure is representative of low-rise buildings regular in plane and in elevation, while the plane eight storeys structure is representative of mid-rise buildings regular in plane and in elevation as well. The plane behaviour is the assumption on which the proposed strategy is based, therefore in the third benchmark structure this assumption has been removed by inserting non-symmetrical infills that produce a strong in-plane irregularity.

For each structural model two levels of the nominal capacity-demand ratio (C/D) in terms of top displacements have been considered, 0.7 and 0.5. The pushover analysis for each of the benchmark structures have been preliminary performed and the bilinear base shear-top displacement has been obtained (Fig. 9). To do this, cross-sections as shown in Figs. 7 and 8 have been assumed and modeled as fiber cross-sections, with the characteristics of the materials shown in Fig. 10. Infills have been modeled as equivalent pin-jointed diagonal struts with a linear indefinitely elastic material consistent with the characteristics of materials used for infills. The bilinear equivalent shear-displacement curves have been chosen so to assign as a limit state the achievement of the maximum stress f_{cc} in the reinforced concrete cross-sections in agreement with Fig. 10 (however, the branch until the deformation capacity ε_{ccu} was necessary to perform the dynamic analyses).

The nominal ratios 0.7 and 0.5 between capacity and demand have been obtained once the response spectrum has been assigned accordingly. To limit the number of spectra to be managed, only two were chosen in such a way that the ratio capacity-demand stayed around 0.5 in one case and around 0.7 in the second case (for this reason, these ratios were defined "nominal"). It was verified, after the bilinear curves were derived, that a response spectrum with PGA of 0.41g and a response spectrum with PGA of 0.46g were appropriate, respectively, to have a nominal ratio capacity-demand of 0.7 and 0.5 for the three benchmark models analyzed.

In both cases, the target spectra derive from the Italian standards [34] but the procedure is not affected by this choice. In Figs. 11 and 12 the acceleration-displacement response spectra used to obtain the capacity-demand ratios before mentioned are inserted and the force-displacement bilinear curves for each benchmark structure are jointly introduced.

In Figs. 11 and 12, for comparison, the bilinear structural responses obtained after pushover analysis and stopped at the assigned ultimate limit state are mass normalized as the response spectra. All the responses are characterized by a fundamental period T in the elastic stage higher

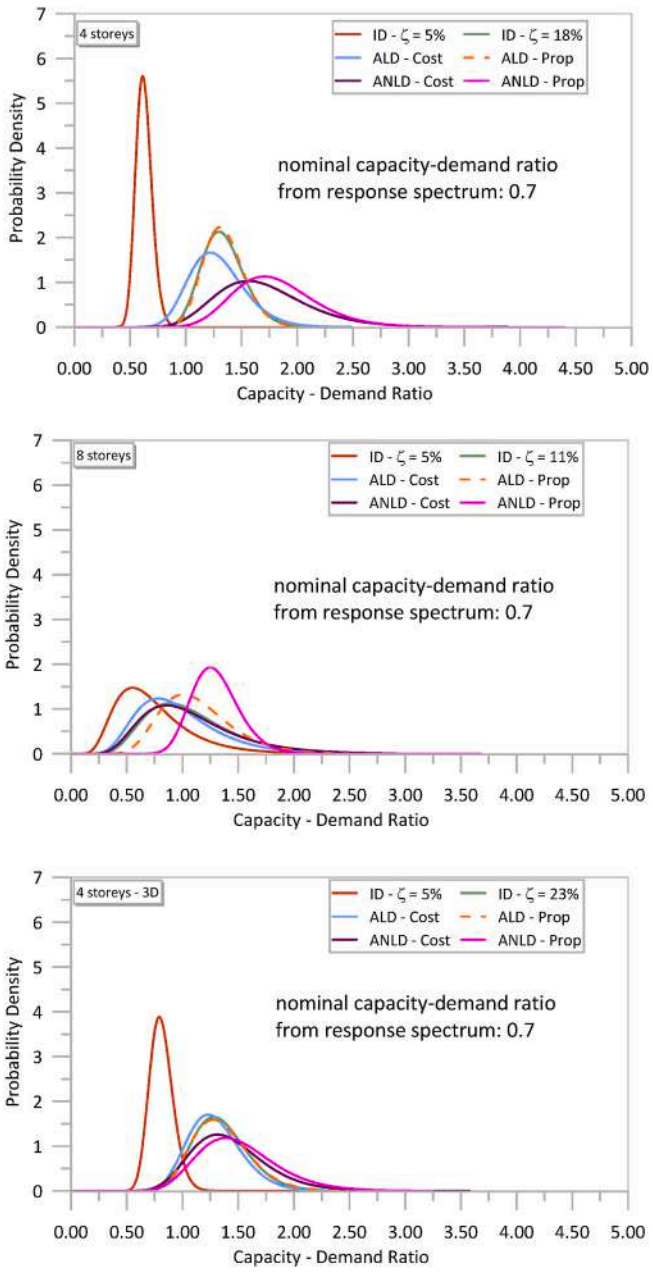

Fig. 14. – Capacity-demand ratio probability density distributions before and after the introduction of the additional damping (ID-$\zeta = 5\%$: original structure with inherent damping 5%; ID-$\zeta = 23\%$: structure with inherent damping 23%; ALD-Cost: linear dampers uniformly distributed in elevation; ANLD-Cost: non-linear dampers uniformly distributed in elevation; ALD-Prop: linear dampers distributed according to the storey shear; ANLD-Prop: non-linear dampers distributed according to the storey shear).

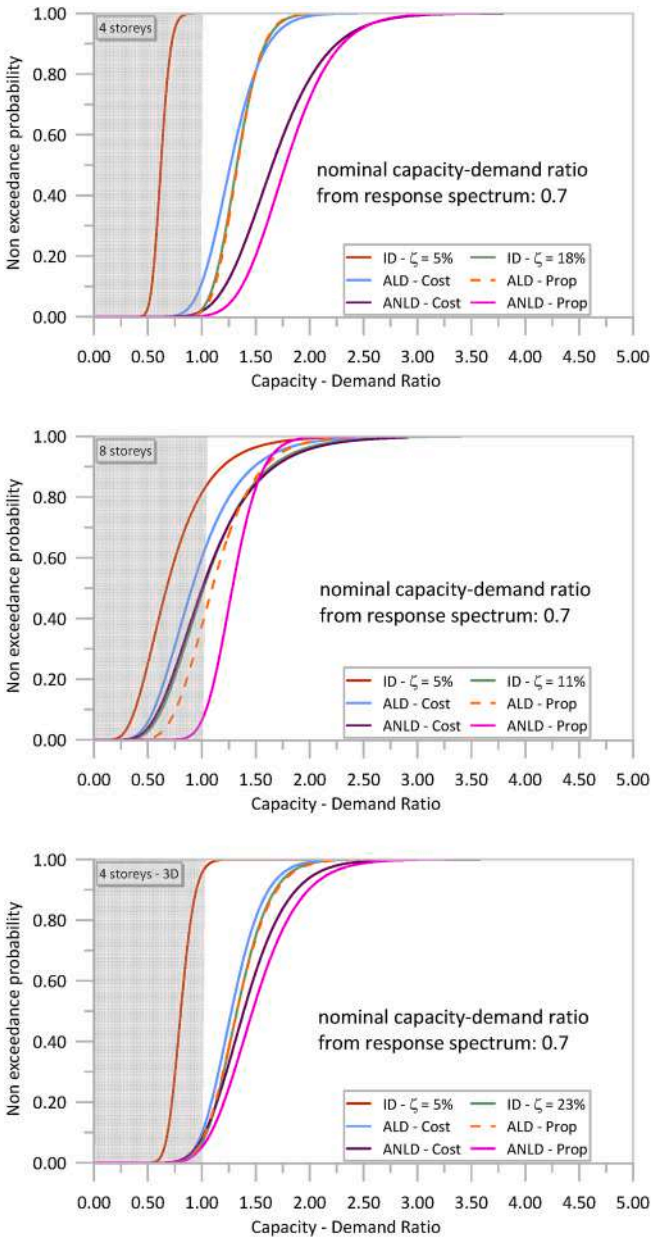

Fig. 15. – Capacity-demand ratio cumulative probability distributions before and after the introduction of the additional damping (legend in caption of Fig. 14).

than T_C, namely the response elastic branch encounters the response spectrum in its third branch.

To this point, 50 accelerograms have been generated compatible with the spectra assigned for the dynamic analyses to be performed before and after the introduction of the fluid viscous dampers. Different strategies are available in the literature for the generation of spectrum compatible accelerograms (eg., Ref. [59]). In this case, natural acceleration time series were made spectrum compatible by using the Time Domain Method first introduced in Ref. [60] and implemented in different software.

In comparison, the uniform damping distribution, the concentrated damper distribution uniform in elevation and the concentrated damper distribution consistent with the distribution of the storey shear have been considered. The cases of use of linear and non-linear dampers have been discussed.

Table 1 provides the values of the additional damping ζ_d obtained by Eqs. (10) and (11) (graphically obtained in Figs. 11 and 12 as well), of the storey dissipation parameters C obtained by Eq. (19), the values C_1 and C_n assigned to the first storey and the top storey in the case of distribution according with the storey shear distribution (Eq. (25)), and finally the corresponding values $C_{1,nl}$ and $C_{n,\,nl}$ obtained by Eq. (29) in the case of non-linear dampers (the effective value $\alpha = 0.15$ of the exponent in Eq. (29) has been fixed in this study). In Table 1, the participation mass associated to the modal shape used for the estimation of the damper parameters has been also inserted.

The assessment of the effectiveness of the proposed simplified procedure was done in a probabilistic sense by observing and processing the results of dynamic analyses from, as before mentioned, 50 accelerograms. As regards the choice of the accelerograms, a selection was done

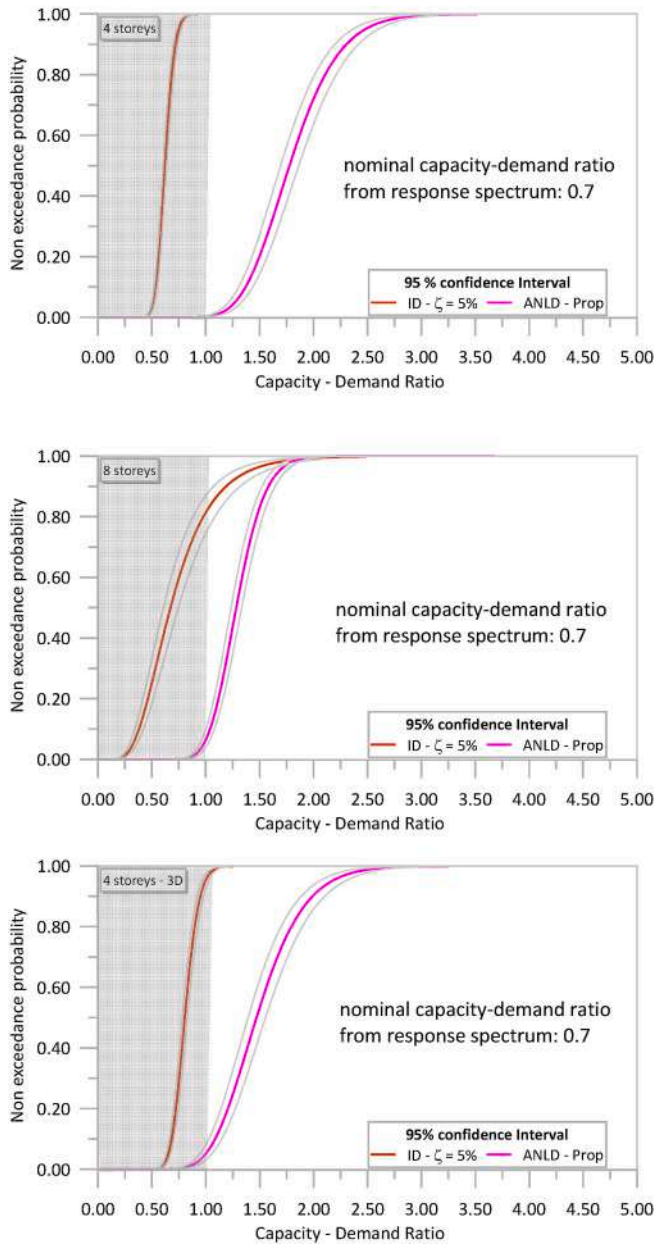

Fig. 16. – Capacity-demand ratios cumulative probability distribution (with 95 % confidence intervals) before and after the introduction of non-linearly non-uniformly distributed dampers (legend in caption of Fig. 14).

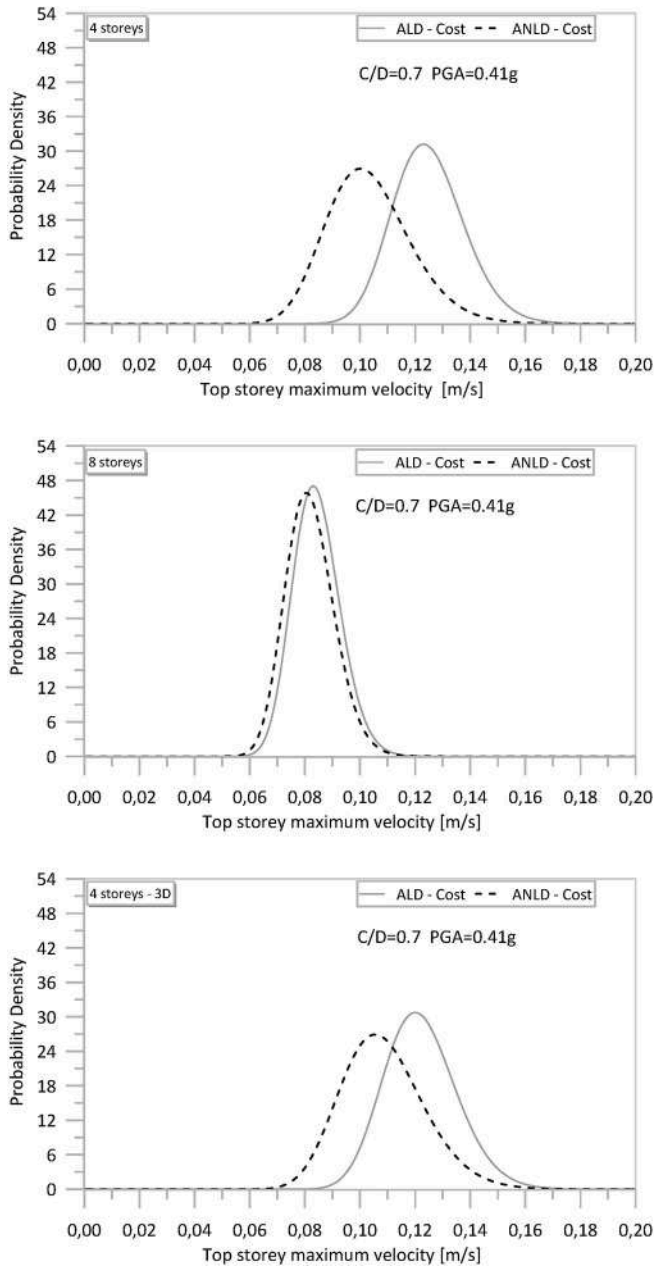

Fig. 17. – Comparison between the distribution of the maximum velocities exhibited by the structures with linear dampers and with equivalent non-linear dampers – C/D = 0.7 - (legend: ALD-Cost: linear dampers uniformly distributed in elevation; ANLD-Cost: non-linear dampers uniformly distributed in elevation).

in such a way the corresponding response spectra provided meanly the PGA associated to each of the two target spectra.

In Fig. 13 a comparison between the target spectra and the spectra from the accelerograms used for the dynamic analyses is proposed.

From each analysis capacity and demand have been extracted with and without additional damping and the probabilistic distributions of the capacity-demand ratios have been calculated and compared.

The additional damping was first considered as inherent damping, then as linear dampers at each storey and finally as non-linear dampers at each storey. In the latter two cases, two different distributions were considered, uniform in elevation and consistent with the storey shear.

For the probabilistic distribution of capacity-demand ratios a lognormal distribution has been assumed. In Table 2, mean and standard deviation of the capacity-demand ratios are inserted for comparison.

In Fig. 14, the capacity-demand distributions obtained in the case of a nominal capacity-demand ratio equal to 0.7 before the intervention are inserted.

What immediately emerges from Fig. 14 is that the most frequent value of capacity-demand ratio obtained from the analyses for the original state structure is higher than the one obtainable by the pushover analysis. It was expected since pushover analysis provides a range for the capacity-demand ratio and, in this study, the lower bound has been considered. Also, non-linear dampers are much more effective than linear dampers, especially if distributed according to the storey shear. This is much more evident in the case of mid-rise structures, where the uniform distribution in elevation, in both linear and non-linear cases, does not cause an appropriate increase in the capacity, leaving approximately a probability of 50% of collapse. This circumstance is much clearer by the observation of the cumulative density functions in Fig. 15.

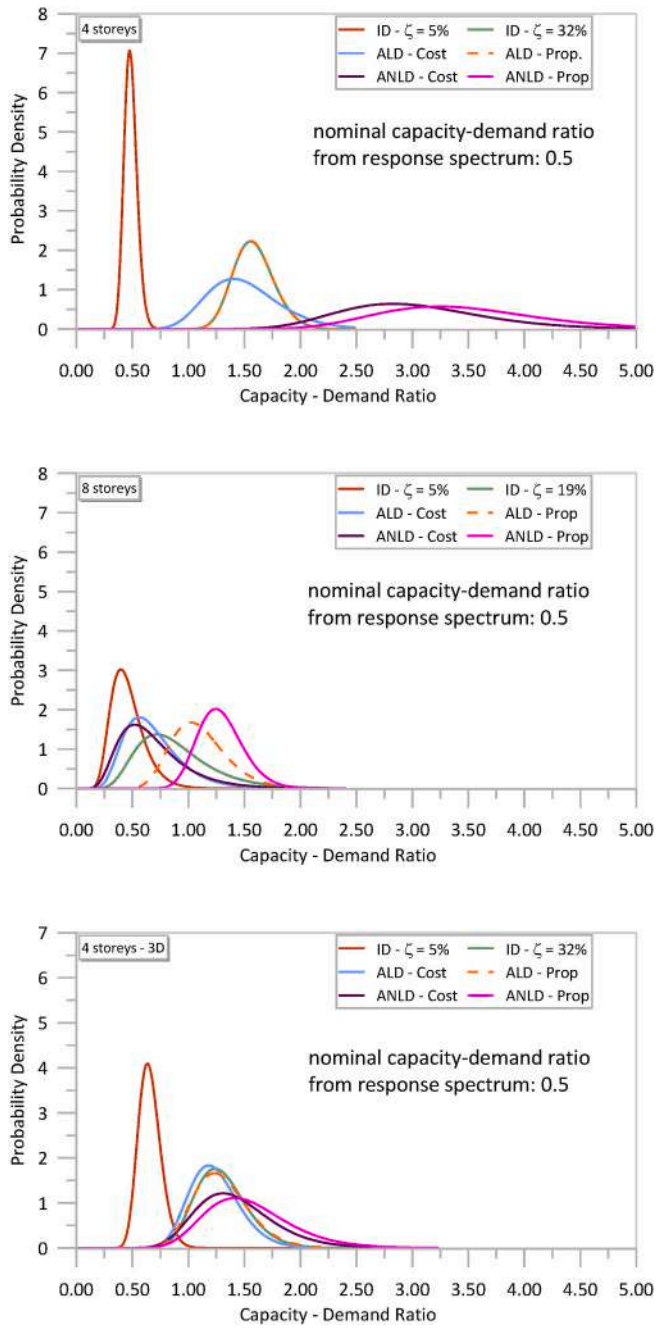

Fig. 18. – Capacity-demand ratio probability density function before and after the introduction of the additional damping (legend in caption of Fig. 14).

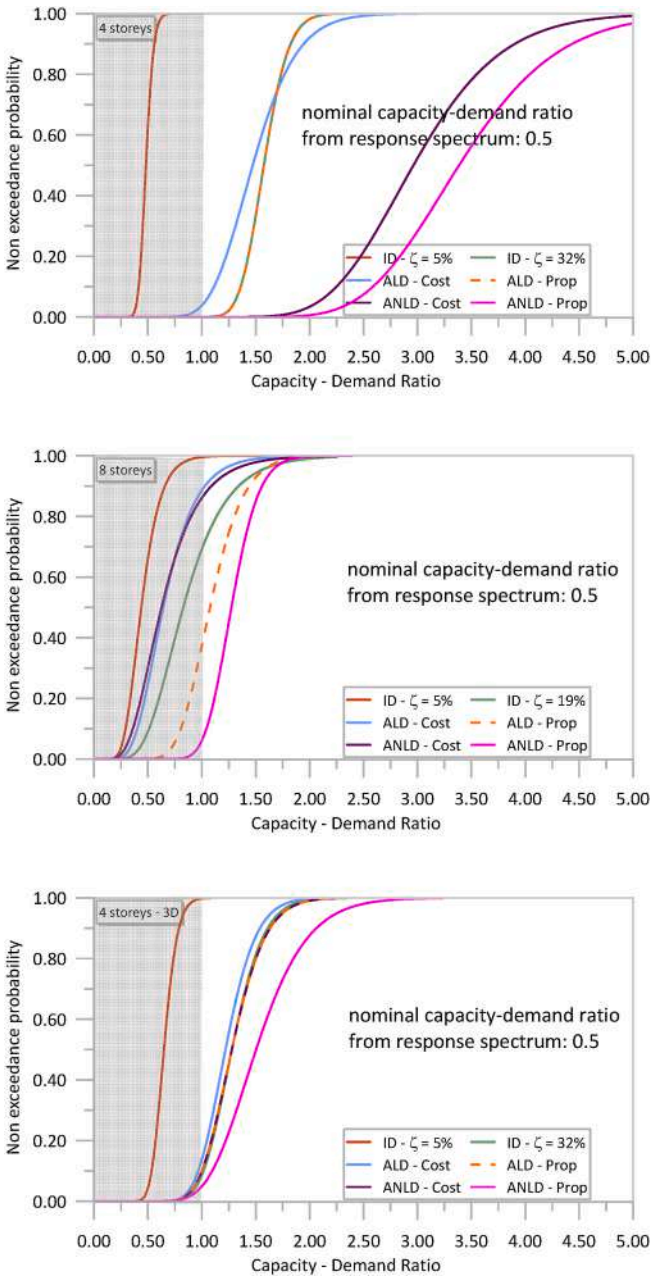

Fig. 19. – Capacity-demand ratio probability density distributions before and after the introduction of the additional damping (legend in caption of Fig. 14).

In fact, only a not uniform distribution of non-linear dampers is able to guarantee always a probability of occurrence lower than 5% for a ratio capacity/demand <1. This is immediately clear by observing the overlapping of the cumulative probability functions and the grey area of the plane non-exceedance probability vs capacity-demand ratio. It is worth observing that there is a difference between the probability distribution of the capacity demand ratios in the case of additional damping attributed as inherent damping to the structure and additional damping attributed as concentrated damping by fluid viscous dampers. This is remarked only to remember that, in the design stage, the additional damping is assumed as inherent distributed damping differently from what done after, that is the introduction of a concentrated damping at each storey.

For the case of low-rise structures, regular or not regular in plan, uniform distributions of the dampers, in linear or non-linear conditions, seem appropriate as the non-uniform distributions of non-linear dampers.

A comparison of the cumulative probability function of the structure capacity-demand ratio in the original state and after the introduction of the non-linear damper with non-uniform distribution in elevation is shown in Fig. 16 where the 95% confidence intervals are included as well.

The slope of the cumulative probability functions in the three cases reveals a higher scatter of the capacity-demand ratio of the structures provided with additional damping capacity with respect to the structure in the original state in the case of low-rise structures but not in the case of mid-rise structures. A more precise observation of the results reveals that this difference is not due to a different standard deviation of the results after the additional damping capacity is introduced but it is the consequence of a higher scatter of the results of the capacity-demand

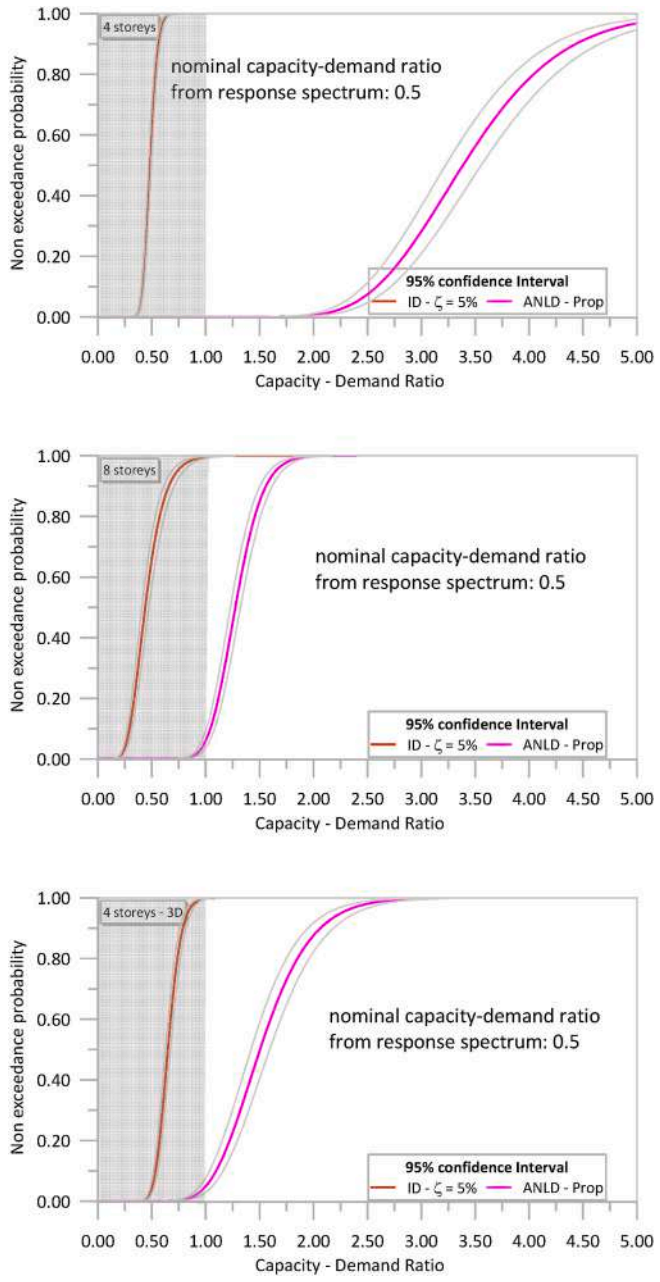

Fig. 20. – Capacity-demand ratios cumulative probability distribution (with 95 % confidence intervals) before and after the introduction of non-linearly non-uniformly distributed dampers (legend in caption of Fig. 14).

ratio in the case of mid-rise structures in the original state. It means that in general the introduction of additional damping capacity reduces and, in a certain sense, aligns the scatter of the responses. As a last issue, it has to be underlined that the reliability of Eq. (29) is decisive for the results. Observe that Eq. (29), as the equations from which it is derived, assumes that the maximum velocity in the dampers is equal in the linear and in the non-linear case. However, this circumstance is not necessarily respected. The equation in question provides a C_{nl} higher in general than the one necessary because the higher efficiency of the non-linear dampers reduces the maximum displacements and velocities.

This is immediately clear from Fig. 17, where a comparison between the distribution of the maximum velocity $|\dot{u}_{n,\max}|$ appearing in Eq. (29), as derived from the analyses on the structures with linear dampers and from the analyses on the structures with non-linear dampers, is shown.

The analyses have been repeated for an initial nominal capacity-demand ratio equal to 0.5 providing results not different from those obtained in the case of a capacity-demand ratio equal to 0.7.

The results in Figs. 18–20 confirm.

What emerges from Figs-18-20 is that, in the case of low-rise plane structures, the procedure seems too much conservative with respect to the objective of the design. However, it is the consequence of the estimation of the maximum velocities by the response spectrum (Eq. (30)), that resulted conservative in each case.

7. Case study

In the previous section, ideal structures under loads and having characteristics of the cross-sections of reinforced concrete members merely assumed have been analyzed with the scope to understand the influence on the proposed procedure that is based on a simplified and specific structural behaviour. In this section, the proposed FVD design strategy is applied to a case study, to provide its reliability in the case of real structures. It is a 3-dimensional structure with a plane behaviour but is able to exhibit a torsional response. The test is considered basic just to check if characteristics that frequently can be found in practical applications may change the results expected by a procedure characterized by simplifications that neglect those characteristics.

The building in object belong to the Cannizzaro hospital complex located in Catania (Sicily). It is intended to outpatient activity. It is a low-rise building symmetric in plane and regular in elevation. The characteristics of the reinforced concrete structure (geometry) are included in (Fig. 21).

An experimental campaign on the materials (concrete and steel of rebars) revealed that the shape of the constitutive laws are consistent with those reported in Fig. 10 but with the level of the mechanical parameters inserted in Table 3.

The pushover analyses have been preliminary performed and the bilinear base shear-top displacement has been obtained (Fig. 22). To do this, cross-sections (Fig. 21) have been assumed as specified in the original project and modeled as fiber cross-sections.

The nominal capacity-demand ratio (C/D) in terms of displacements has been obtained once the response spectrum has been assigned, according to the site parameters and building characteristics. It was obtained C/D = 0.56.

The target spectrum derives from the Italian standards [34] but the procedure is not affected by this choice. In Fig. 23 the acceleration-displacement response spectrum used to obtain the capacity-demand ratio before mentioned is inserted and the force-displacement bilinear curve for the structure is jointly introduced.

In Fig. 23, for comparison, the bilinear structural response obtained after pushover analyses and stopped at the assigned ultimate limit state (corresponding to the achieving of the reinforced concrete strength f_{cc}) is mass normalized as the response spectrum. The response is characterized by a fundamental period T in the elastic stage higher than T_C, namely the response elastic branch encounters the response spectrum in its third branch.

Dynamic analyses have been performed before and after the introduction of the fluid viscous dampers using 50 accelerograms (in Fig. 24 the response spectra compared with a target spectrum can be found). In the comparisons an increased inherent damping, a concentrated damper distribution uniform in elevation and a concentrated damper distribution consistent with the distribution of the storey shear have been considered. The cases of use of linear and non-linear dampers have been discussed.

The following Table 4 provides the values of the additional damping ζ_d obtained by Eqs. (10) and (11) (graphically obtained in Fig. 23 as well), of the storey dissipation parameters C obtained by Eq. (19), the values C_1 and C_n assigned to the bottom storey and the top storey in the case of distribution according with the storey shear distribution (Eq. (25)), and finally the corresponding values $C_{1,nl}$ and $C_{n,\,nl}$ obtained by Eq. (29) in the case of non-linear dampers (the effective value $\alpha = 0.15$ of

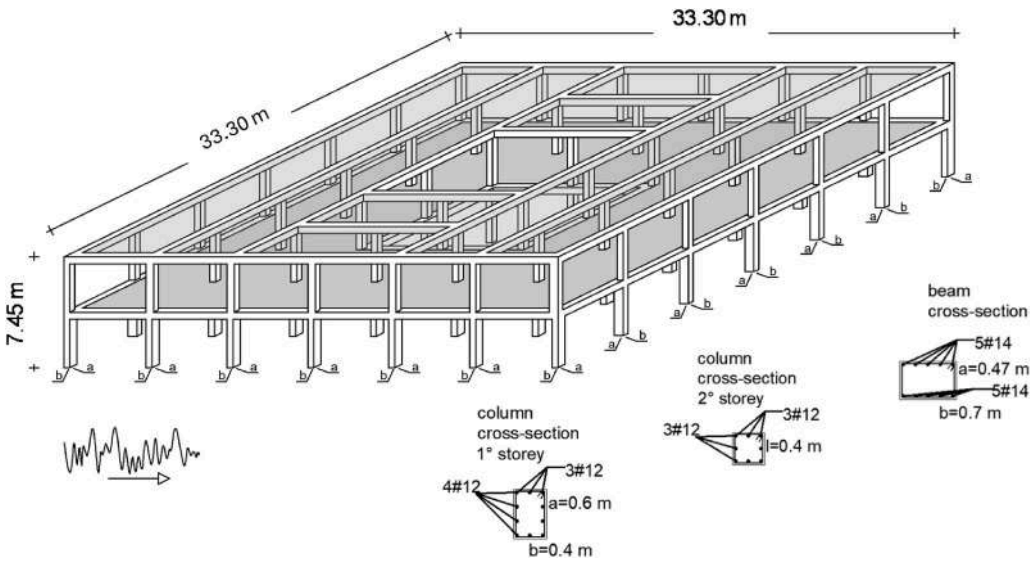

Fig. 21. – Structure of one of the buildings of the Cannizzaro hospital complex in Catania (Sicily).

Table 3
– Mechanical characteristics obtained by laboratory test.

Concrete			
f_{cc}	27 MPa	ε_{cc}	0.0015
E_c	18530 MPa	ε_{cu}	0.005
Steel			
f_{sy}	366 MPa	ε_{sy}	0.0021
f_{su}	493 MPa	ε_{su}	0.675

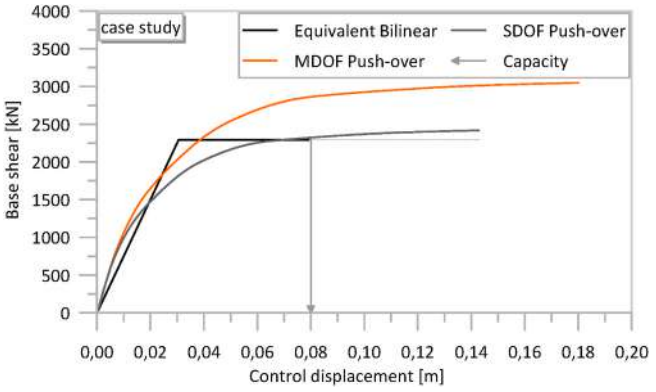

Fig. 22. – Capacity curves of the case study structure in agreement to N2 method (C/D = 0.56).

the exponent in Eq. (29) has been fixed in this study). In Table 4, the participation mass associated to the modal shape used for the estimation of the damper parameters has been also inserted. In Table 5 mean and standard deviation of the capacity-demand ratios in the original state and after the introduction of FVDs are inserted.

In Fig. 25, the capacity-demand ratio probability distribution obtained in the case of nominal capacity-demand ratio equal to 0.56 before the intervention is inserted together with the capacity-demand ratios probability distribution obtained after the introduction of fluid viscous dampers in different configurations.

What emerges in this case study (Fig. 25) is that the most frequent value of capacity-demand ratio obtained from the analyses for the original state structure is almost equal to the one obtainable by the pushover analysis, often used in practical applications to study existing

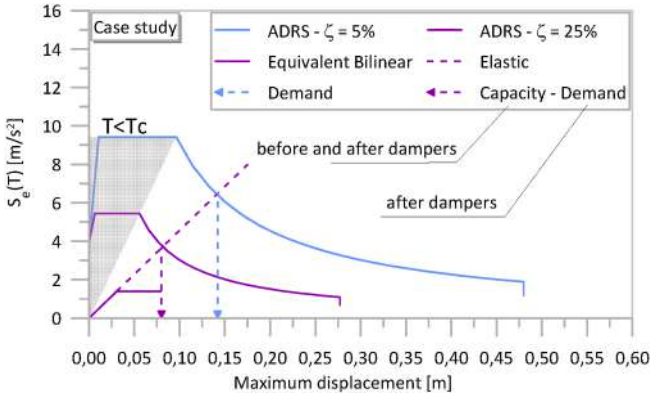

Fig. 23. – Bilinear structural response (mass normalized) and acceleration-displacement response spectra (PGA = 0.40g) before (ζ = 5%) and after the introduction of fluid viscous dampers; nominal Capacity-Demand Ratio in the original state equal to 0.56.

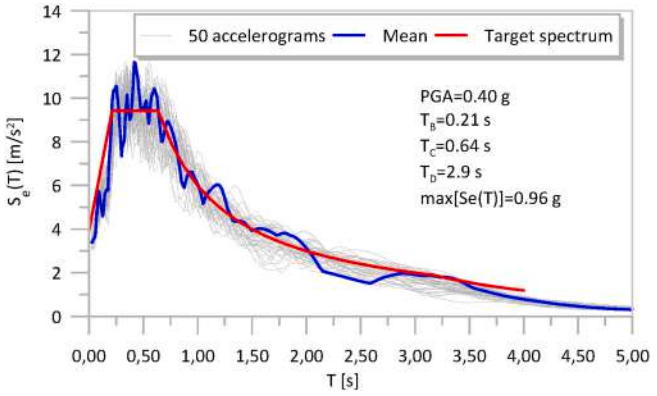

Fig. 24. – Comparison between target spectrum and spectrum of the accelerograms used for the dynamic analyses (target spectrum parameters in figure).

structures behaviour. Also, non-linear dampers are much more effective than linear dampers as expected after the investigation on the benchmark systems, but without any relevant advantages if distributed according to the storey shear. This result is absolutely consistent with the

Table 4
– Values of the additional damping ζ_d and the corresponding FVDs' parameters, and the participation mass associated to the modal shape used for the design.

	ζ_d [%]	$C_{lc}\left[kN\cdot\frac{s}{m}\right]$		$C_{nlc}\left[kN\cdot\left(\frac{s}{m}\right)^{0.15}\right]$
Case study	20	1383		474
$C_{lp}\left[kN\cdot\frac{s}{m}\right]$		$C_{nlp}\left[kN\cdot\left(\frac{s}{m}\right)^{0.15}\right]$		Modal participating Mass Ratios
Lower Storey	Upper Storey	Lower Storey	Upper Storey	
1828	937	627	321	83%

results obtained from the benchmark structure (4-storey plane structure) representing the class of low-rise buildings with plane behaviour. So, the results have a double value: the first one is the validation of the design strategy and the second one is the validation of the choice of a 4-storey plane structure as the benchmark of the class of low-rise buildings with plane behaviour. This circumstance is much clearer by the observation of the cumulative density functions in Fig. 26.

Once again, Fig. 26 shows a difference between the probability distribution of the capacity demand ratios in the case of additional damping attributed as inherent damping to the structure and additional damping attributed as concentrated damping by fluid viscous dampers. This is remarked only to remember that, in the design stage, the additional damping is assumed as inherent distributed damping differently from what done after by the use of FVDs.

A comparison of the cumulative probability function of the structure capacity-demand ratio in the original state and after the introduction of the non-linear damper with non-uniform distribution in elevation is shown in Fig. 27 where the 95% confidence intervals are included as well.

The slope of the cumulative probability functions reveals a higher scatter of the capacity-demand ratio of the structure provided with additional damping capacity respect to the structure in the original state, as in the case of low-rise structures.

Also in this case, as in the study of the benchmark systems, it is possible to give evidence of the non-reliability of Eq. (29) where the maximum velocities in the system with linear FVDs are assumed equal to the velocities with non-linear FVDs. This is immediately clear from Fig. 28, where a comparison between the distribution of the maximum velocity $|\dot{u}_{n,\max}|$ appearing in Eq. (29), as derived from the analyses on the structure with linear dampers and from the analyses on the structure with non-linear dampers, are shown. However, this is not a reason to not use Eq. (29) by means of that conservative results can be obtained in any case.

8. Conclusions

Fluid viscous dampers (FVDs) can be a good seismic protection system for existing buildings. FVDs can really provide an additional important energy dissipation capability that, coupled with the natural capability of structural systems to dissipate by hysteresis mechanisms and by the inherent viscosity, is a solution to seismic demand.

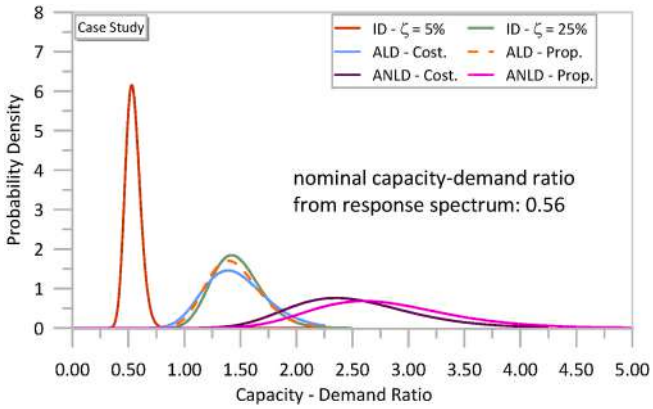

Fig. 25. – Capacity-demand ratio probability density distributions before and after the introduction of the additional damping (legend: ID-ζ = 5%: original structure with inherent damping 5%; ID-ζ = 25%: structure with inherent damping 25%; ALD-Cost: linear dampers uniformly distributed in elevation; ANLD-Cost: non-linear dampers uniformly distributed in elevation; ALD-Prop: linear dampers distributed according to the storey shear; ANLD-Prop: non-linear dampers distributed according to the storey shear).

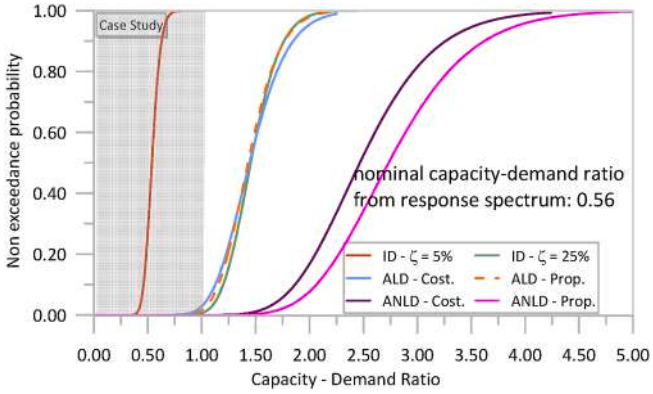

Fig. 26. – Capacity-demand ratio cumulative probability distributions before and after the introduction of the additional damping (legend in caption of Fig. 25).

Missing a specific simplified design strategy for FVDs in reinforced concrete framed structures that, cannot renounce to the possibility to dissipate by hysteresis, and the possibility of exhibiting a non-linear behaviour and local plasticization, in this study a novel approach is proposed combining the fundamentals of the N2 method and the correlation between indefinitely linear systems and elastic-plastic systems (characterized by the same stiffness in the elastic stage) in terms of displacement seismic demand.

The proposed procedure assumes the linear behaviour of the FVDs, the plane behaviour of the structure and the uniform distribution of the dampers in elevation in terms of dissipation capability to be converted by a specific strategy, after the first stage of the design, in a non-uniform distribution of non-linear dampers.

Table 5
– Mean and standard deviation of the capacity-demand ratios obtained from 50 dynamic analyses.

			Capacity/Demand	
			mean	standard deviation
Case Study	Inherent Damping (5%)	C/D = 0.56 from N2 method	0,541	0,069
	Additional Inherent Damping (20%)		1,470	0,206
	linear FVDs – uniform distribution		1,467	0,250
	nonlinear FVDs – uniform distribution		2,527	0,562
	linear FVDs – storey shear distribution		1,447	0,220
	nonlinear linear FVDs – storey shear distribution		2,800	0,602

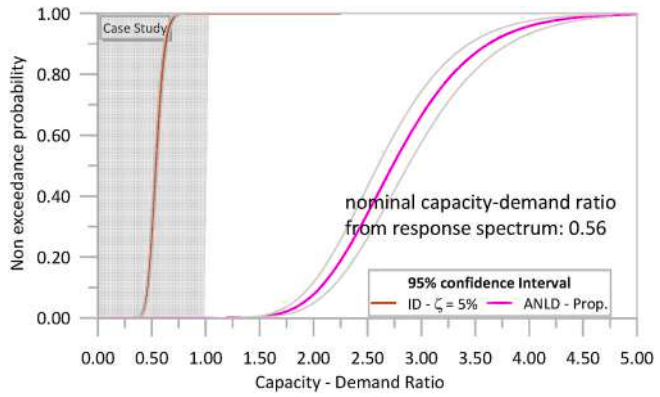

Fig. 27. – Capacity-demand ratios cumulative probability distribution (with 95 % confidence intervals) before and after the introduction of non-linearly non-uniformly distributed dampers (legend in caption of Fig. 26).

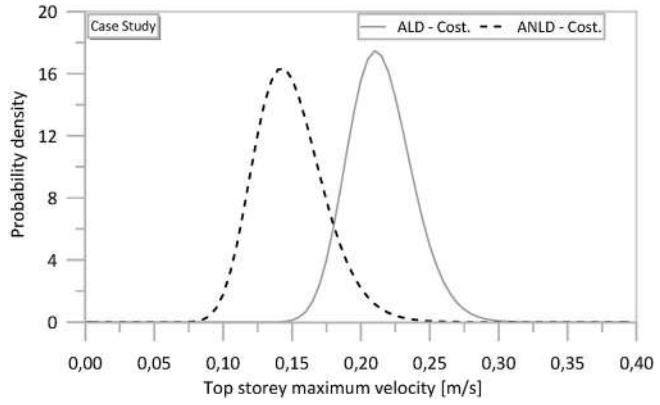

Fig. 28. – Comparison between the distribution of the maximum velocities exhibited by the structures with linear dampers and with equivalent non-linear dampers.

The reliability of the proposed approach has been checked by the probabilistic point of view by observing the dynamic responses of benchmark structures under families of accelerograms matching specific target spectra, in two cases of nominal capacity-demand ratios (C/D) as derived by the N2 method (C/D = 0.5 and C/D = 0.7), and observing the dynamic response of a real structure equipped with FVDs as obtained by the proposed approach. In the present study, the classes of low-rise plane-like behaviour structures, mid-rise plane-like behaviour structures and low-rise irregular-in-plan structures have been investigated to extend to other further classes. The proposed procedure requests as input the capacity-demand ratio as obtained by the N2 method.

The approach proposed and the observation of the results obtainable by its use has revealed that:

1) For each class, the proposed approach provides a solution, in terms of distribution and capacity of non-linear fluid viscous dampers, able to guarantee at least a 95% of probability to obtain a capacity-demand ratio higher than 1;
2) In the case of low-rise buildings, the proposed approach provides a 95 % of probability to obtain a capacity-demand ratio higher than one just with linear fluid viscous dampers uniformly distributed (in terms of dissipating capacity) in elevation; a 100% probability to have C/D > 1 is obtained just converting linear dampers in non-linear dampers by the principle of the equivalent dissipated energies over a cycle force-displacement;
3) In the case of mid-rise and in-plane non-regular buildings, converting linear dampers in non-linear dampers and distributing the dissipation capacity proportionally to the storey shear guarantee obtaining the probability of success stated at previous bullet 1;
4) The not different results obtained for the class of in-plane non-regular buildings prove that the simplified assumptions on which the FVDs are designed do not take away from an optimal solution and do not reduce the probability of success;
5) In each case, the results prove that considering the additional damping that a structure needs as an inherent damping, instead of concentrated damping as in reality, does not affect the probability of success; this derives from the closeness of the probability density functions obtained in the two configurations of additional inherent damping and concentrated damping provided by FVDs;
6) The simplicity of the approach proposed and the characteristics of the approach itself suggest an extension to the case of classes of structures with different characteristics from those investigated; it is referred to steel structures as irregular elevation (r.c. or steel) structures.

CRediT authorship contribution statement

Anthea Amato: Writing – review & editing, Writing – original draft, Methodology, Investigation, Formal analysis, Data curation, Conceptualization. **Liborio Cavaleri:** Writing – review & editing, Writing – original draft, Validation, Methodology, Investigation, Funding acquisition, Formal analysis, Data curation, Conceptualization.

Declaration of competing interests

Declare that they have no known competing financial interests or personal relationships that could have appeared to influence the work reported in this paper.

Acknowledgments

This study was carried out within the RETURN Extended Partnership and received funding from the European Union Next-GenerationEU (National Recovery and Resilience Plan – NRRP, Mission 4, Component 2, Investment 1.3 – D.D. 1243 August 2, 2022, PE0000005)

References

[1] X. Liu, W. Wang, J. Li, Full-scale shaking table tests and numerical studies of structural frames with a hybrid isolation system, Eng. Struct. 292 (2023) 116545, https://doi.org/10.1016/j.engstruct.2023.116545.
[2] C. Li, Y. Liu, H.-N. Li, Fragility assessment and optimum design of a steel–concrete frame structure with hybrid energy-dissipated devices under multi-hazards of earthquake and wind, Eng. Struct. 245 (2021) 112878, https://doi.org/10.1016/j.engstruct.2021.112878.
[3] R. Ullah, M. Vafaei, S.C. Alih, A. Waheed, A replaceable sandwiched metallic fuse damper for seismic protection of braced frames, Eng. Struct. 298 (2024) 117072, https://doi.org/10.1016/j.engstruct.2023.117072.
[4] A. Benavent-Climent, E. Oliver-Saiz, J. Donaire-Ávila, Seismic retrofitting of RC frames combining metallic dampers and limited strengthening with FRP/SRP applying energy-based methods, Soil Dynam. Earthq. Eng. 177 (2024) 108432, https://doi.org/10.1016/j.soildyn.2023.108432.
[5] G. Terenzi, Energy-based design criterion of dissipative bracing systems for the seismic retrofit of frame structures, Appl. Sci. 8 (2018) 268, https://doi.org/10.3390/app8020268.
[6] S. Sorace, G. Terenzi, Seismic protection of frame structures by fluid viscous damped braces, J. Struct. Eng. 134 (2008) 45–55, https://doi.org/10.1061/(ASCE)0733-9445(2008)134:1(45).
[7] E. Parcianello, C. Chisari, C. Amadio, Optimal design of nonlinear viscous dampers for frame structures, Soil Dynam. Earthq. Eng. 100 (2017) 257–260, https://doi.org/10.1016/j.soildyn.2017.06.006.
[8] M.D. Martínez-Rodrigo, J. Lavado, P. Museros, Dynamic performance of existing high-speed railway bridges under resonant conditions retrofitted with fluid viscous dampers, Eng. Struct. 32 (2010) 808–828, https://doi.org/10.1016/j.engstruct.2009.12.008.
[9] Y.-X. Hui, L.-S. Li, H. Cheng, Y.-J. Zhang, D.-S. Wang, Seismic mitigation of continuous girder bridges equipped with U-Shaped stainless steel dampers under near-fault earthquake excitations, Struct 58 (2023) 105597, https://doi.org/10.1016/j.istruc.2023.105597.

[10] W.-H. Feng, Z.-M. Xu, S. Yin, J.-X. Sun, B.-L. Zheng, S.-J. Wang, Weathering steel damper and its application: a case study for double-column piers, Soil Dynam. Earthq. Eng. 173 (2023) 108160, https://doi.org/10.1016/j.soildyn.2023.108160.
[11] X. Xu, X. Chen, H. Hu, X. Zhou, M. Cheng, L. Sun, X. Li, Energy dissipation and seismic response reduction system for high-speed railway bridges based on multiple performance requirements, Eng. Struct. 307 (2024) 117919, https://doi.org/10.1016/j.engstruct.2024.117919.
[12] L. Su, W. Zhang, Y. Chen, C. Zhang, Seismic design and shaking table test of continuous girder bridges with winding rope fluid viscous dampers, Eng. Struct. 277 (2023) 115408, https://doi.org/10.1016/j.engstruct.2022.115408.
[13] J. Fu, S. Wan, P. Zhou, J. Shen, M. Loccufier, K. Dekemele, Effect of magnetic-spring Bi-Stable nonlinear energy sink on vibration and damage reduction of concrete double-column piers: experimental and numerical analysis, Eng. Struct. 303 (2024) 117517, https://doi.org/10.1016/j.engstruct.2024.117517.
[14] C. Wu, H. Jing, Z. Feng, J. Song, T. Wan, Z. Chen, Control of longitudinal movement response of suspension bridges induced by passing trains using low-exponent fluid viscous dampers, Struct 62 (2024) 106330, https://doi.org/10.1016/j.istruc.2024.106330.
[15] J. Li, L. Xu, Seismic performance improvement of continuous rigid-frame bridges with hybrid control system under near-Fault ground motions, Soil Dynam. Earthq. Eng. 168 (2023) 107858, https://doi.org/10.1016/j.soildyn.2023.107858.
[16] J. Zhu, S.-J. Jiang, Z. Xiong, M. Wu, Y. Li, Longitudinal vibration control strategy for long-span suspension bridges under operational and extreme excitations using eddy current dampers, Struct 58 (2023) 105603, https://doi.org/10.1016/j.istruc.2023.105603.
[17] K.V. Sharma, V. Parmar, L. Gautam, S. Choudhary, J. Gohil, Modelling efficiency of fluid viscous dampers positioning for increasing tall buildings' resilience to earthquakes induced structural vibrations, Soil Dynam. Earthq. Eng. 173 (2023) 108108, https://doi.org/10.1016/j.soildyn.2023.108108.
[18] R. Hu, S. Hu, M. Yang, Y. Zhang, Metallic yielding dampers and fluid viscous dampers for vibration control in civil engineering: a review, Int. J. Struct. Stabil. Dynam. 22 (2022) 2230006, https://doi.org/10.1142/S0219455422300063.
[19] T. Guo, J. Xu, W. Xu, Z. Di, Seismic upgrade of existing buildings with fluid viscous dampers: design methodologies and case study, J. Perform. Constr. Facil. 29 (2015) 04014175, https://doi.org/10.1061/(ASCE)CF.1943-5509.0000671.
[20] K.Y.M. Almajhali, Review on passive energy dissipation devices and techniques of installation for high rise building structures, Struct 51 (2023) 1019–1029, https://doi.org/10.1016/j.istruc.2023.03.025.
[21] M.D. Symans, F.A. Charney, A.S. Whittaker, M.C. Constantinou, C.A. Kircher, M. W. Johnson, R.J. McNamara, Energy dissipation systems for seismic applications: current practice and recent developments, J. Struct. Eng. 134 (2008) 3–21, https://doi.org/10.1061/(ASCE)0733-9445(2008)134:1(3).
[22] M.F. Ferrotto, L. Cavaleri, Variable Friction Dampers (VFD) for a modulated mitigation of the seismic response of framed structures: characteristics and design criteria, Probab. Eng. Mech. 70 (2022) 103375, https://doi.org/10.1016/j.probengmech.2022.103375.
[23] M.F. Ferrotto, M. Di Paola, L. Cavaleri, Seismic behavior of structures equipped with variable friction dissipative (VFD) systems, Bull. Earthq. Eng. 19 (11) (2021) 4623–4639, https://doi.org/10.1007/s10518-021-01116-x.
[24] L. Cavaleri, F. Di Trapani, M.F. Ferrotto, Experimental determination of viscous damper parameters in low velocity ranges, Int. J. Earthq. Eng. 34 (2) (2017) 64–74.
[25] R. Siami Kaleybar, P. Tehrani, Effects of using different arrangements and types of viscous dampers on seismic performance of intermediate steel moment frames in comparison with different passive dampers, Struct 33 (2021) 3382–3396, https://doi.org/10.1016/j.istruc.2021.06.079.
[26] M.S. Sebaq, Y. Zhou, G. Song, Y. Xiao, Plastic energy evaluation of bilinear SDOF systems with fluid viscous dampers, Struct. Des. Tall Spec. 32 (2023) e2011, https://doi.org/10.1002/tal.2011.
[27] Y. Zhou, X. Lu, D. Weng, R. Zhang, A practical design method for reinforced concrete structures with viscous dampers, Eng. Struct. 39 (2012) 187–198, https://doi.org/10.1016/j.engstruct.2012.02.014.
[28] K. Kasai, M. Nishijima, K. Tanaka, S. Wang, S. Mahin, Simplified design method for frames with nonlinear viscous dampers, in: Proceedings of the Eleventh US National Conference on Earthquake Engineering, 2018. Los Angeles.
[29] D. Patsialis, A.A. Taflanidis, A. Giaralis, Exploring the impact of excitation and structural response/performance modeling fidelity in the design of seismic protective devices, Eng. Struct. 291 (2023) 115811, https://doi.org/10.1016/j.engstruct.2023.115811.
[30] S. Sanghai, C. Gurmule, Seismic response control of RCC building with plan and vertical irregularities using dampers, J. Build. Rehabil. 9 (2024) 9, https://doi.org/10.1007/s41024-023-00358-3.
[31] N. Gluck, A.M. Reinhorn, J. Gluck, R. Levy, Design of supplemental dampers for control of structures, J. Struct. Eng. 122 (1996) 1394–1399, https://doi.org/10.1061/(ASCE)0733-9445(1996)122:12(1394).
[32] D. De Domenico, G. Ricciardi, I. Takewaki, Design strategies of viscous dampers for seismic protection of building structures: a review, Soil Dynam. Earthq. Eng. 118 (2019) 144–165, https://doi.org/10.1016/j.soildyn.2018.12.024.
[33] Federal Emergency Management Agency (FEMA) and American Society of Civil Engineers (ASCE), Prestandard and Commentary for the Seismic Rehabilitation of Buildings, November 2000. Report FEMA-356, Washington, DC.
[34] Ministero Infrastrutture e Trasporti, Aggiornamento Delle Norme Tecniche per Le Costruzioni (NTC 2018 - Italian Technical Standard for Construction), 2018.
[35] N. Impollonia, A. Palmeri, Seismic performance of buildings retrofitted with nonlinear viscous dampers and adjacent reaction towers, Earthq. Eng. Struct. Dynam. 47 (5) (2018) 1329–1351, https://doi.org/10.1002/eqe.3020.
[36] S. Wang, S.A. Mahin, High-performance computer-aided optimization of viscous dampers for improving the seismic performance of a tall building, Soil Dynam. Earthq. Eng. 113 (2018) 454–461, https://doi.org/10.1016/j.soildyn.2018.06.008.
[37] L. Cavaleri, M. Di Paola, Statistic moments of the total energy of potential systems and application to equivalent non-linearization, Int. J. Non Lin. Mech. 35 (4) (2000) 573–587, https://doi.org/10.1016/S0020-7462(99)00020-7.
[38] L. Cavaleri, M. Di Paola, G. Failla, Some properties of multi-degree-of-freedom potential systems and application to statistical equivalent non-linearization, Int. J. Non Lin. Mech. 38 (3) (2003) 405–421, https://doi.org/10.1016/S0020-7462(01)00080-4.
[39] G. Navarra, F. Lo Iacono, M. Oliva, An efficient stochastic linearisation procedure for the seismic optimal design of passive control devices, Front. Built Environ. 6 (2020) 32, https://doi.org/10.3389/fbuil.2020.00032.
[40] G. Navarra, F. Lo Iacono, M. Oliva, Probabilistic optimal design of passive control devices coherently with seismic codes response spectra, in: Proc. of XXIII Conference of the Italian Association of Theoretical and Applied Mechanics (Aimeta), September 2017, pp. 4–7. Salerno, Italy.
[41] M. Donà, E. Bernardi, A. Zonta, P. Tan, F. Zhou, Evaluation of optimal FVDs for inter-storey isolation systems based on surrogate performance models, Bull. Earthq. Eng. 19 (2021) 4587–4621, https://doi.org/10.1007/s10518-021-01134-9.
[42] G. Asadpour, P. Asadi, R. Garcia, I. Hajirasouliha, A novel stochastic linearization technique for structures with nonlinear fluid viscous dampers including soil-structure interaction, J. Build. Eng. 72 (2023) 106668, https://doi.org/10.1016/j.jobe.2023.106668.
[43] N. Pollini, Simultaneous analysis and design optimization for seismic retrofitting of hysteretic structures with fluid viscous dampers, J. Build. Eng. 87 (2024) 109123, https://doi.org/10.1016/j.jobe.2024.109123.
[44] D. Altieri, E. Tubaldi, E. Patelli, A. Dall'Asta, Assessment of optimal design methods of viscous dampers, Procedia Eng. 199 (2017) 1152–1157, https://doi.org/10.1016/j.proeng.2017.09.286.
[45] A. Rodríguez-Castellanos, M. Niño, S.E. Ruiz, M.A. Santos Santiago, Multi-disciplinary performance comparison for selecting the optimal sustainable design of buildings structures with fluid-viscous dampers, Soil Dynam. Earthq. Eng. 178 (2024) 108450, https://doi.org/10.1016/j.soildyn.2024.108450.
[46] S. Silvestri, T. Trombetti, Physical and numerical approaches for the optimal insertion of seismic viscous dampers in shear-type structures, J. Earthq. Eng. 11 (5) (2007) 787–828, https://doi.org/10.1080/13632460601034155.
[47] O. Lavan, G.F. Dargush, Multi-objective evolutionary seismic design with passive energy dissipation systems, J. Earthq. Eng. 13 (6) (2009) 758–790, https://doi.org/10.1080/13632460802598545.
[48] H. Movaffaghi, O. Friberg, Optimal placement of dampers in structure using genetic algorithm, Eng. Comput. 23 (6) (2006) 597–606, https://doi.org/10.1108/02644400610680324.
[49] J.N. Yang, S. Lin, J. Kim, A.K. Agrawal, Optimal design of passive energy dissipation systems based on H∞ and H2 performances, Earthq. Eng. Struct. Dynam. 31 (2002) 921–936, https://doi.org/10.1002/eqe.130.
[50] S.S. Ijmulwar, S.K. Patro, Seismic design of reinforced concrete buildings equipped with viscous dampers using simplified performance-based approach, Struct 61 (2024) 106020, https://doi.org/10.1016/j.istruc.2024.106020.
[51] M. Palermo, S. Silvestri, L. Landi, G. Gasparini, T.A. Trombetti, Direct five-step procedure for the preliminary seismic design of buildings with added viscous dampers, Eng. Struct. 173 (2018) 933–950, https://doi.org/10.1016/j.engstruct.2018.06.103.
[52] M. Marra, M. Palermo, S. Silvestri, The direct five-step procedure for the design of added viscous dampers to be inserted into existing buildings: formulation and case study, Front. Built Environ. 9 (2023) 1289851, https://doi.org/10.3389/fbuil.2023.1289851.
[53] S. Moradpour, M. Dehestani, Optimal DDBD procedure for designing steel structures with nonlinear fluid viscous dampers, Struct 22 (2019) 154–174, https://doi.org/10.1016/j.istruc.2019.08.005.
[54] P. Fajfar, The story of the N2 method, IAEE, Tokio, Japan (2021).
[55] G. Alotta, L. Cavaleri, M. Di Paola, M.F. Ferrotto, Solution for the design and increasing of efficiency of fluid viscous dampers, Open Construct. Build Technol. J. 10 (Suppl. 1) (2016) 106–121.
[56] N. Pollini, O. Lavan, O. Amir, Minimum-cost optimization of nonlinear fluid viscous dampers and their supporting members for seismic retrofitting, Earthq. Eng. Struct. Dynam. 46 (12) (2017) 1941–1961.
[57] Federal Emergency Management Agency (FEMA) and American Society of Civil Engineers (ASCE), Guidelines for the Seismic Rehabilitation of Buildings, October 1997. Report FEMA-273, Washington, DC.
[58] Federal Emergency Management Agency (FEMA) and American Society of Civil Engineers (ASCE), Commentary on the Guidelines for the Seismic Rehabilitation of Buildings, October 1997. Report FEMA-274, Washington, DC.
[59] G. Barone, F. Lo Iacono, G. Navarra, A. Palmeri, Closed-form stochastic response of linear building structures to spectrum-consistent seismic excitations, Soil Dynam. Earthq. Eng. 125 (2019) 105724, https://doi.org/10.1016/j.soildyn.2019.105724.
[60] K. Lilhanand, W.S. Tseng, Development and application of realistic earthquake time histories compatible with multiple-damping design spectra, in: Proceeding of the 9th World Conference on Earthquake Engineering, 1988. Tokyo-Kyoto, Japan.